Alma Mater Studiorum – Università di Bologna

DOTTORATO DI RICERCA IN

Scienze Biomediche

Ciclo 27

Settore Concorsuale di afferenza: 06/A4

Settore Scientifico disciplinare: MED/08

THE CONSTITUTIVE ACTIVATION OF THE DNA DAMAGE RESPONSE PATHWAY IS A NOVEL THERAPEUTIC TARGET IN AGGRESSIVE B-CELL LYMPHOMA.

Presentata da: **Dr. Enrico Derenzini**

Coordinatore Dottorato **Relatore**

Prof. Lucio Ildebrando Cocco **Prof. Stefano Pileri**

Esame finale anno 2015

Table of Contents

Abstract

The recent finding that *MYC*-driven cancers are sensitive to inhibition of the DNA damage response (DDR) pathway, prompted us to investigate the role of DDR pathway as therapeutic target in diffuse large B-cell lymphoma (DLBCL), which frequently overexpresses the *MYC* oncogene. In a preliminary immunohistochemical study conducted on 99 consecutive DLBCL patients, we found that about half of DLBCLs showed constitutive expression of the phosphorylated forms of checkpoint kinases (CHK) and CDC25c, markers of DDR activation, and of phosphorylated histone H2AX (γH2AX), marker of DNA damage and genomic instability. Constitutive γH2AX expression correlated with c-MYC levels and DDR activation, and defined a subset of tumors characterised by poor outcome. Next, we used the CHK inhibitor PF-0477736 as a tool to investigate whether the inhibition of the DDR pathway might represent a novel therapeutic approach in DLBCL. Submicromolar concentrations of PF-0477736 hindered proliferation in DLBCL cell lines with activated DDR pathway. These results were fully recapitulated with a different CHK inhibitor (AZD-7762). Inhibition of checkpoint kinases induced rapid DNA damage accumulation and apoptosis in DLBCL cell lines and primary cells. These data suggest that pharmacologic inhibition of DDR through targeting of CHK kinases may represent a novel therapeutic strategy in DLBCL.

The second part of this work is the clinical, molecular and functional description of a paradigmatic case of primary refractory Burkitt lymphoma characterized by spatial intratumor heterogeneity for the *TP53* mutational status, high expression levels of genomic instability and DDR activation markers, primary resistance to chemotherapy and exquisite sensitivity to DDR inhibitors.

PART I

Introduction

Diffuse large B cell lymphoma (DLBCL), the most common non Hodgkin lymphoma (NHL) subtype, is characterized by an aggressive clinical course [1], and standard first line R-CHOP (Rituximab, Cyclophosphamide, Doxorubicin, Vincristine, Prednisone) chemoimmunotherapy results in approximately 60% cure rates [2].

In the last ten years gene expression profiling has identified two distinct signatures strongly related to the outcome and response to therapy, the germinal center (GCB) B-cell and the activated B-cell (ABC) signatures [3-5], but this classification did not translate yet in a tailored therapeutic approach, as the International prognostic index (IPI) risk score (based on clinical variables), remains the most reliable prognostic tool available in clinical practice [2]. Interestingly, recent data show that a significant fraction of DLBCL display chromosomal segregation defects and aneuploidy, a prominent feature of instable genomes, and these characteristics have been demonstrated to correlate with poor prognosis following conventional R-CHOP chemoimmunotherapy [6]. Accordingly, whole exome sequencing studies showed that DLBCLs are characterized by a particularly large number of genomic aberrations [7]. Moreover a consistent percentage of DLBCLs are characterized by increased c-MYC expression [8-10] which is linked mechanistically to instrinsic genomic instability by a mechanism called replicative stress, consisting in DNA damage accumulation during the S phase of the cell cycle [11].

Genomic instability is now considered a hallmark of cancer, which indicates a tendency toward accumulation of DNA damage with progressive acquisition of mutations and genomic abnormalities, favouring cancer development, metastatic phenotypes and chemoresistance [11,12]. Following DNA damage, cells normally respond by activating the DNA damage repair pathway (DDR), which results in cell cycle arrest, DNA repair or eventually p53-mediated cell death [13]. The ataxia telangiectasia mutated (ATM) and ataxia telangiectasia and RAD3-related protein (ATR) kinases are activated following DNA double and/or single strand breaks and in turn they

phosphorylate the downstream targets checkpoint kinases (CHK) 1 and 2, and the histone H2AX, which is considered to be a reliable DNA damage marker [13-15]. CHK1 and CHK2 activation triggers the inhibitory phosphorylation of the CDC25 phosphatases, which results in delayed mitotic entry, ensuring appropriate DNA repair at the G2/M checkpoint [13].

Accordingly it has been recently demonstrated that tumours bearing high levels of oncogene-induced replicative stress, such as *MYC* driven aggressive lymphoma mouse models and neuroblastoma, are sensitive to single agent CHK inhibitors [16-18].

On the other hand recent studies show that a subset of DLBCLs display mutations of genes involved in DNA repair [19]. Although the functional consequences of specific mutations have not been elucidated yet, these data further highlight the role of the DDR pathway in DLBCL pathogenesis. Therefore, inhibition of the DNA damage repair pathway may represent a valid therapeutic approach to fight cancers with aberrant DDR activation and CHK inhibitors are currently being tested in clinical trials in combination with DNA damaging agents (chemotherapy and radiotherapy) in a variety of tumors [20,21]. Taken together these findings represent a strong rationale to investigate the functional role of the DDR pathway in DLBCL, and to ascertain whether its components might represent potential therapeutic targets. Here we demonstrated that 1) a substantial fraction of DLBCLs display constitutive expression of the DNA damage marker γH2AX, which was associated with poor prognosis following conventional R-CHOP/CHOP-like chemoimmunotherapy, 2) that c-MYC expression, γH2AX and DDR activation were significantly associated, confirming the intimate relationship between oncogene–induced genomic instability and DDR activation in DLBCL, and 3) that DLBCL cell lines and primary cells exhibiting constitutive activation of the DDR pathway are very sensitive to the inhibition of checkpoint kinases. Taken together these data suggest that pharmacologic inhibition of DDR through targeting of CHK kinases may represent a new promising therapeutic strategy in the subset of DLBCLs with activated DDR pathway.

RESULTS

Constitutive activation of DDR components and genomic instability in diffuse large B-cell lymphomas.

We assessed by immunohistochemistry the expression levels of the components of the DDR pathway (CHK1, CHK2, CDC25c) and their phosphorylated forms in three reactive lymphnodes, 27 cases of small lymphocyte lymphoma (SLL), 18 marginal zone lymphoma (MZL), 44 Hodgkin lymphoma (HL), 22 Burkitt lymphoma (BL), and 99 consecutive DLBCL cases diagnosed at our Institution from 2002 to 2011.

Components of the DDR pathway CHK1, CHK2 and CDC25c resulted to be expressed in 100% of B cell neoplasms and normal reactive follicles tested (Table 1) but only aggressive lymphomas (BLs and DLBCLs) showed a significant activation of DDR pathway, as demonstrated by the expression of CHK1, phosphorylated at ser 345, and CDC25c, phosphorylated at ser 216 (Table 1). The phosphorylated form of the CHK2 kinase at thr 68 was found to be expressed only in a minority of DLBCL cases (5%) (Table 1).

We thus hypothesized that lymphomas with constitutive activation of the DDR pathway would be characterized by higher levels of inherent genomic instability.In order to verify this hypothesis we investigated the expression of the phosphorylated form of the histone H2AX at serine 139 (γH2AX), a marker of DDR activation and DNA double strand breaks [13-15], in our B-cell lymphoma panel. Remarkably DLBCLs showed the highest constitutive γH2AX expression with 47% of positive cases (defined as percentage of positive cells ≥30%, in the methods section), confirming that DLBCL is a neoplasm characterized by high genomic instability and inherent DNA damage (Figure 1A,B). Reactive follicles and indolent B-cell lymphomas (MZL and CLL) showed low or absent expression of activated DDR components and γH2AX, and Hodgkin lymphoma cases showed intermediate expression (18% of γH2AX positive cases) (Table 1, Figure 1A,B).

By using cluster analysis on immunohistochemical results, considering the whole panel of DDR activation markers, aggressive B-cell neoplasms (DLBCL and BL) clearly clustered together, being characterized by higher constitutive CHK1, CDC25c, and H2AX phosphorylation, whereas indolent B-cell neoplasms and HL formed a separate cluster (Figure 1A).

Since high inherent genomic instability favours cancer progression and chemoresistance we next investigated the prognostic significance of constitutive γH2AX expression and DDR activation in DLBCL patients. All patients were diagnosed and treated with chemoimmunotherapy at our institution. Characteristics of patients and univariate analyses are shown in table 2. The spectrum of γH2AX expression is shown in figure 1C. In the univariate analysis, pCDC25c ser 216 and γH2AX overexpression were significantly associated with worse overall survival (Table 2), as well as age≥60 years, IPI score>2 and bcl-2/MYC double positivity. Remarkably 5-year OS was 41% for γH2AX positive vs 70% for γH2AX negative patients (Figure 1D). Interestingly, the prognostic significance of γH2AX was particularly evident in the low-intermediate risk IPI group (0-2 risk factors), identifying a subgroup characterized by worse outcome (55% 5-year OS) (Figure 1E). In the multivariate framework γH2AX was found to be an independent prognostic predictor (Table 3). These results suggest that constitutive γH2AX expression is an independent negative prognostic predictor in DLBCL, being able to identify patients with poor prognosis even within the low-intermediate risk group according to the IPI score.

Table 1. Immunohistochemical results.

Tumor type	CHK1		pCHK1		CHK2		pCHK2		CDC25		pCDC25		γH2AX	
	pos	(%)	pos	(%)	pos	(%)	pos	(%)	pos	(%)	pos	(%)	pos	(%)
RL	3/3	(100)	0/3	(0)	3/3	(100)	0/3	(0)	3/3	(100)	0/3	(0)	0/3	(0)
CLL/SLL	27/27	(100)	2/27	(7)	27/27	(100)	0/27	(0)	27/27	(100)	0/27	(0)	3/27	(11)
SMZL	18/18	(100)	2/18	(11)	18/18	(100)	0/18	(0)	18/18	(100)	0/18	(0)	1/18	(5)
CHL	44/44	(100)	6/44	(14)	44/44	(100)	3/44	(7)	44/44	(100)	9/44	(20)	8/44	(18)
BL	22/22	(100)	10/22	(45)	22/22	(100)	3/22	(14)	22/22	(100)	18/22	(82)	5/22	(23)
DLBCL	99/99	(100)	38/99	(38)	99/99	(100)	5/99	(5)	99/99	(100)	40/99	(40)	47/99	(47)

Abbreviations: positive (pos), negative (neg), reactive lymph nodes (RL), chronic lymphocytic leukaemia/small lymphocyte lymphoma (SLL), marginal zone lymphomas (MZL), classical Hodgkin lymphoma (CHL), Burkitt lymphoma (BL), diffuse large B –cell lymphomas (DLBCL).

Fig. 1

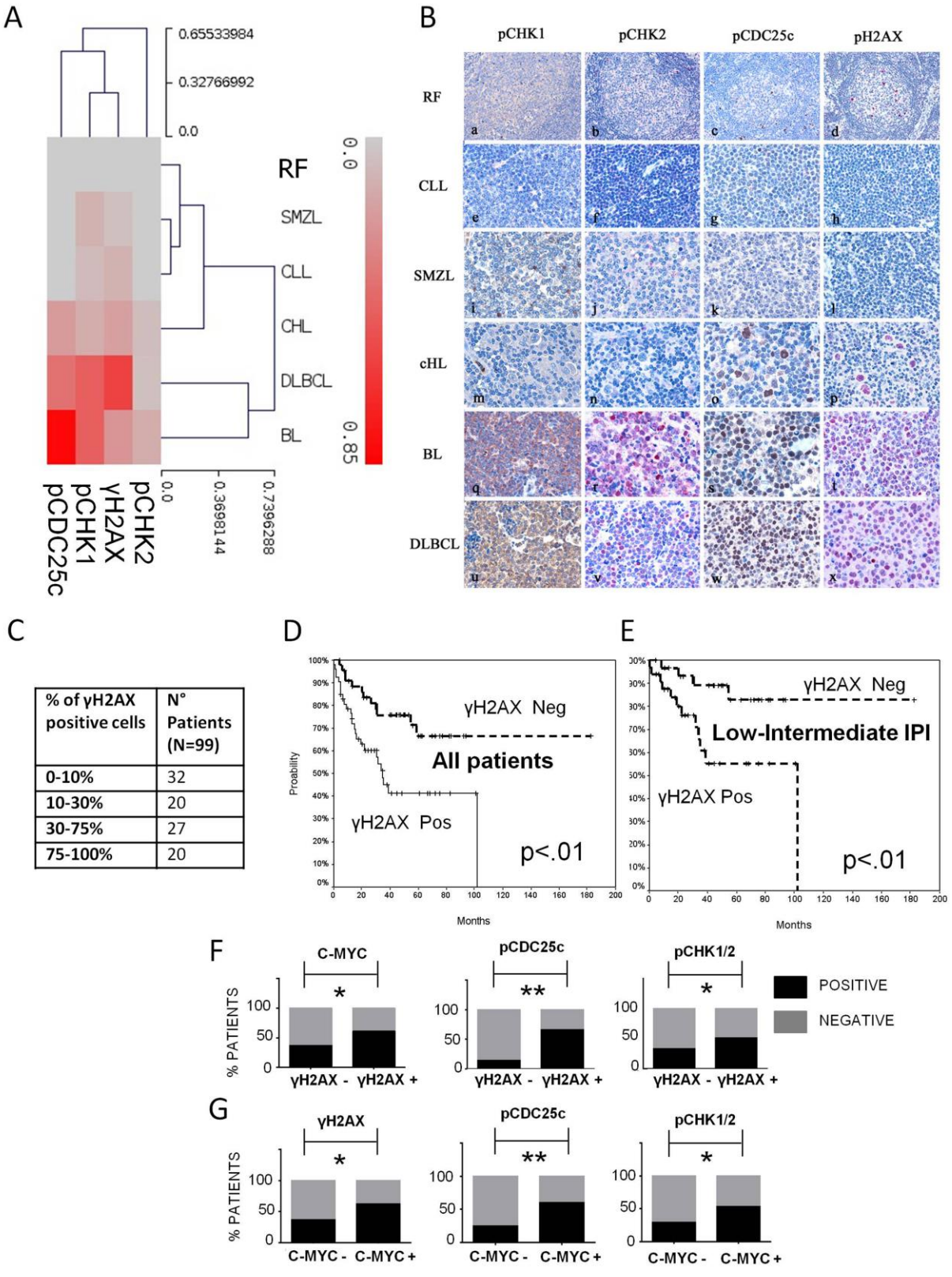
A
0.65533984
0.32766992
0.0
RF
SMZL
CLL
CHL
DLBCL
BL
0.0
0.85
0.0
0.3698144
0.7396288
pCDC25c
pCHK1
γH2AX
pCHK2
B
pCHK1
pCHK2
pCDC25c
pH2AX
RF
CLL
SMZL
cHL
BL
DLBCL
C
% of γH2AX positive cells
N° Patients (N=99)
0-10%
32
10-30%
20
30-75%
27
75-100%
20
D
γH2AX Neg
All patients
γH2AX Pos
p<.01
Proability
Months
E
γH2AX Neg
Low-Intermediate IPI
γH2AX Pos
p<.01
Months
F
C-MYC
pCDC25c
pCHK1/2
POSITIVE
NEGATIVE
% PATIENTS
γH2AX -
γH2AX +
G
γH2AX
pCDC25c
pCHK1/2
% PATIENTS
C-MYC -
C-MYC +

Figure 1. The DDR pathway is aberrantly active in DLBCL.

A) Hierarchical clustering, displayed in a dendrogram, showing higher constitutive activation of the DDR pathway and γH2AX staining in aggressive non Hodgkin B-cell lymphomas (DLBCL and BL), compared to indolent B-cell lymphoma subtypes (CLL, SMZL), HL and reactive follicles (RF) . The level of expression in each lymphoma type and in RF, that is the number of positive cases/number of evaluable cases, is represented by a color scale, starting from grey, indicating 0% of the samples positive, up to brilliant red, indicating 85% of the samples positive (the maximum percentage of positivity detected was 82%). The highest levels of γH2AX and pCHK1ser 345 staining were observed in DLBCL, with 47% and 38% of cases expressing respectively γH2AX and pCHK1 ser 345 in more than 30% of cells.

B) Representative TMA spots of reactive follicles (RF) (a-d), CLL (e-h), SMZL (i-l) HL (m-p), BL (q-t) and DLBCL (u-x) stained for pCHK1, pCHK2, pCDC25c and γH2AX. Higher expression levels of activated DDR pathway components and γH2AX were observed in DLBCL and BL, compared to indolent NHL subtypes and HL, showing low or absent DDR activation and γH2AX staining.

C) Table showing the spectrum of γH2AX expression in our DLBCL cohort.

D) Overall survival (OS) curve of γH2AX positive compared to γH2AX negative DLBCL patients. 99 consecutive DLBCL patients diagnosed and treated at our institution with Rituximab plus CHOP/CHOP-like regimens from 2002 to 2011 were considered. Patients positive (pos) for γH2AX at initial diagnosis had a significant inferior OS rates compared to γH2AX negative (neg) ones (with 5-year OS rate of 41% vs 70% respectively, $p<0.01$, log-rank test).

E) Overall survival curve of the low-intermediate risk IPI group according to the γH2AX status. 63 patients with low-intermediate risk IPI score (0-2) were considered in this subgroup analysis. The 5-year OS of γH2AX positive patients resulted significantly lower compared to the OS of γH2AX negative patients, with 5-year OS rate of 55% vs 83% respectively ($p<0.01$, log-rank test).

F) Bar graphs showing a significantly increased incidence of c-MYC, pCDC25c, and pCHK1/2 positive cases in the γH2AX positive subgroup, compared to the γH2AX negative subgroup.

The incidence of c-MYC positive cases raised from 35% to 62%, from the γH2AX negative to γH2AX positive group ($p=0.02$) (Fisher`s exact test). $^{*}P<0.05$; $^{**}P<0.005$.

The incidence of pCDC25c positive cases increased from 17% to 66% from the γH2AX negative to the γH2AX positive group ($p<0.001$) (Fisher`s exact test).

The incidence of pCHK1/2 positive cases increased from 33% to 51% from the γH2AX negative to the γH2AX positive group (p=0.04) (Fisher`s exact test).

G) Bar graphs showing a significantly increased incidence of γH2AX, pCDC25c, and pCHK1/2 positive cases in the c-MYC positive subgroup, compared to the c-MYC negative subgroup. The 3 cases with missing c-MYC values were excluded from this analysis.

Table 2. Patients characteristics and univariate analyses for overall survival.

Factor	**Patient N°**	**P value**
Gender M F	 58 41	0.75
Median Age (range) < 60 y ≥ 60 y	65 (16-87) 37 62	**0.002**
Cell of Origin GCB Non-GCB	 46 53	0.72
R-CHOP vs R-Other (VNCOP-B/MACOP-B)	67 vs 32	0.16
Ki-67 0-90% ≥ 90%	 66 33	0.6
IPI 0-2 ≥3	 63 36	**<0.001**
p53 0-50% ≥ 50%	 74 23 (2 missing [÷])	0.65
Bcl-2 0-70% ≥ 70%	 28 71	0.052
c-MYC 0-40% ≥ 40%	 49 47 (3 missing [§])	0.46
Bcl-2/MYC Bcl-2/MYC negative Bcl-2/MYC positive	 61 35 (3 missing [§])	**0.03**
pCHK1/2 0-30% ≥ 30%	 58 41	0.06
PCDC25c 0-30% ≥ 30%	 59 40	 **0.02**
pH2AX 0-30% ≥ 30%	 52 47	 **0.01**

÷ Immunohistochemistry data for p53 expression were available for 97 patients; § Immunohistochemistry data for c-MYC expression were available for 96 patients.
Abbreviations: M (male), F (female); VNCOP-B (VP-16, Mitoxantrone, Cyclophosphamide, Vincristine, Prednisone, Bleomycin); MACOP-B (Methotrexate, Doxorubicin, Cyclophosphamide, Vincristine, Prednisone, Bleomycin)., N (number).

Table 3. Multivariate analyses for overall survival.

Factor	**N Patients (n=96)**	**P value**	**Hazard ratio (95%C.I.)**
Age		**0.02**	
<60	36		1
>60	60		2.97 (1.19-7.35)
IPI		**<0.001**	
0-2	61		1
≥ 3	35		3.72 (1.82-7.57)
Bcl-2/MYC		0.12	
Negative	61		-
Positive	35		
pCDC25c		0.26	
Negative	57		-
Positive	39		
γH2AX		**0.01**	
Negative	51		1
Positive	45		2.44 (1.19-4.99)

P value was calculated according to the Cox Regression model.

c-MYC, γH2AX and DDR activation markers are frequently co-expressed in DLBCL

Since it has been reported that *MYC*-driven replicative stress leads to inherent DNA damage [11,12,17,18], we evaluated the correlation between c-MYC, γH2AX (marker of DNA damage) and pCHK1/2 (pCHK1+pCHK2) and pCDC25c expression (markers of DDR activation), hypothesizing that γH2AX positive DLBCLs would be characterized by c-MYC overexpression and enhanced DDR activation.

The 99 patients considered in the survival analysis were divided in 2 groups based on γH2AX expression levels. By using Fisher`s exact test we found a statistically significant association between γH2AX positivity, c-MYC expression, and increased activation of CDC25c and CHK kinases (Figure 1F) (Table 4). Interestingly non-GCB and GCB cases, low and high risk IPI score patients were equally distributed in the γH2AX positive and negative groups (Table 4).

Also by categorizing patients in 2 groups depending on the c-MYC expression status, we could confirm the association between c-MYC, γH2AX, pCDC25c and pCHK1/2 kinases expression: of note γH2AX positive cases raised from 37% to 63%, pCHK1/2 positive cases from 28% to 55%, pCDC25c positive cases from 24% to 55% from the c-MYC negative to the c-MYC positive group (Figure 1G). These results indicate a tight association between c-MYC expression, inherent genomic instability, and constitutive DDR activation.

Table 4. Characteristics of γH2AX negative and positive DLBCL patients with respect to IPI score, p53 expression levels, cell of origin (GCB vs non-GCB), Bcl-2 expression, c-MYC expression, and DDR pathway activation (pCHK1/2, pCDC25c).

Factor	**γH2AX- (N=52)**	**γH2AX+ (N=47)**	**Missing**	**p-value (Fisher`s exact test)**
IPI Low (0-2) High (3-4)	 34 (65%) 18 (35%)	 29 (62%) 18 (38%)	0	0.67
p53 <50% ≥50%	 42 (81%) 9 (17%)	 32 (68%) 14 (30%)	2 (2%)	0.16
Ki-67 <90% ≥90%	 35 (67%) 17 (33%)	 31 (66%) 16 (34%)	0	0.82
Cell of Origin GCB Non-GCB	 26 (50%) 26 (50%)	 20 (43%) 27 (57%)	0	0.45
Bcl-2 <70% ≥70%	 15 (29%) 37 (71%)	 13 (28%) 34 (72%)	0	0.89
c-MYC <40% ≥40%	 31 (60%) 18 (35%)	 18 (38%) 29 (62%)	3 (3%)	**0.01**
pCHK1/2 <30% ≥30%	 35 (67%) 17 (33%)	 23 (49%) 24 (51%)	0	**0.04**
pCDC25c <30% ≥30%	 43 (83%) 9 (17%)	 16 (34%) 31 (66%)	**0**	**<0.001**

P value was calculated with the Fisher`s exact test.

Inhibition of checkpoint kinases hinders proliferation and promotes apoptotic death in DLBCL cells.

The observation that about half of the DLBCL cases were characterised by constitutive γH2AX expression, which was associated with adverse outcome and with activation of the DDR pathway, suggests that inhibition of the DDR may represent a promising new therapeutic strategy to fight this subset of tumours.

Therefore, we explored the effect of DDR pathway inhibition in a series of human B-cell NHL cell lines, including 6 DLBCL cell lines, 1 BL and 1 HL cell line (used respectively as a positive and negative control for constitutive DDR activation). All the DLBCL cell lines, irrespectively of their GC or ABC origin, and the BL cell line RAMOS showed some activation of the DDR pathway, as defined by constitutive phosphorylation of CHK1 at ser 345 and/or phosphorylation of CHK2 at thr 68, and constitutive expression of γH2AX, evaluated by Western blot analysis.

The HL cell line KMH2 showed low or absent basal levels of activation of the DDR pathway, which did not translate in increased γH2AX expression (Figure 2A). In line with the results of the immunohistochemical study, we found a significant correlation between c-MYC levels and pCHK1 ser 345 levels (Figure 2B). Finally, primary cells from 2 out of 3 aggressive B-cell lymphoma patients (2 DLBCL, 1 BL) showed constitutive γH2AX expression. We did not find γH2AX overexpression in indolent B-cell lymphoma primary cells and normal bone marrow mononucleated cells (Figure 2C).

To evaluate the therapeutic potential of CHK inhibition, we incubated B-cell lymphoma cell lines with increasing concentrations of PF-0477736 from 5 nM to 10 μM. Cell viability was assessed by WST-1 assay (Roche). PF-0477736 is a selective ATP competitive CHK inhibitor with IC50 of 2 and 47 nM respectively for CHK1 and CHK2, which was demonstrated to have activity in preclinical models of solid tumours in combination with DNA damaging agents [22,23]. PF-0477736 induced cell death in a time and dose dependent manner, with a maximal effect after 48 hours. The most sensitive cell line was BJAB, with an IC50 of 48 nM and 9nM at 24 and 48 hours (hrs) respectively

(Figure 2 D,E). KM-H2 cells were resistant. All the other DLBCL cell lines were sensitive to nanomolar concentrations of PF-0477736, with IC50s ranging from 160 to 230 nM (Figure 2D,E). The resistant KM-H2 cells did not display any constitutive expression of γH2AX and pCHK2, and only weak pCHK1 and c-MYC expression (Figure 2A). These results were confirmed also by using a different inhibitor of CHK kinases, AZD-7762 [24], which also displayed submicromolar IC50 values at 48 hours (Fig 3) in DLBCL and BL cell lines. Taken together these observations indicate a high efficacy of CHK inhibitors against DLBCL cell lines characterized by constitutive activation of the DDR pathway.

Since some reports link the sensitivity to CHK inhibition to the dysfunction of the p53 axis in different tumor models [22,24], we profiled our cell lines by conventional Sanger sequencing for the presence of *TP53* mutations and *CDKN2A* deletions, (known recurrent genomic alterations in DLBCL which result in p53 axis and G1/S checkpoint dysfunction). Alterations resulting in G1/S checkpoint dysfunction were found in all the DLBCL cell lines and in the BL cell line RAMOS and only the resistant KM-H2 cells were *TP53* wild type with no alteration of *CDKN2A* (Figure 2E) (Table 5). Notably, in line with previous reports [22,24], co-treatment with the CHK inhibitor PF-0477736 enhanced the efficacy of doxorubicin in the *TP53* mutant DLBCL cell lines (Figure 4A).

In order to establish the relevance of p53 status in the cytotoxic activity of PF-0477736, we induced stable transfection of the *TP53* wild-type KM-H2 cells with the dominant negative mutant p53dd. Interestingly we failed to induce sensitivity to PF-0477736 single agent or in combination with doxorubicin after p53dd transfection (Figure 4 B-D). These results indicate that at least in this cellular context disruption of p53 function is not sufficient to induce sensitivity to CHK inhibition or to combinations with doxorubicin, and that probably other mechanisms cooperate in determining the sensitivity to CHK inhibition and dependence on the G2/M checkpoint in these cells.

To further investigate the mechanisms of action of PF-0477736 we determined the effect on apoptosis by using Annexin V/Propidium Iodide staining. In line with WST-1 assay results, low nanomolar concentrations of PF-0477736 induced cell death by apoptosis after 24 hours of incubation in the sensitive BJAB cells, but not in the resistant KM-H2 cells (Figure 5A,B).

Consistent with the induction of apoptosis PARP cleavage was detected by western blot after 24 hours in BJAB cells (Figure 5C).

Nanomolar concentrations of PF-0477736 induced apoptotic cell death also in the other DLBCL cell lines tested at 48 hours (Figure 5D).

Fig. 2

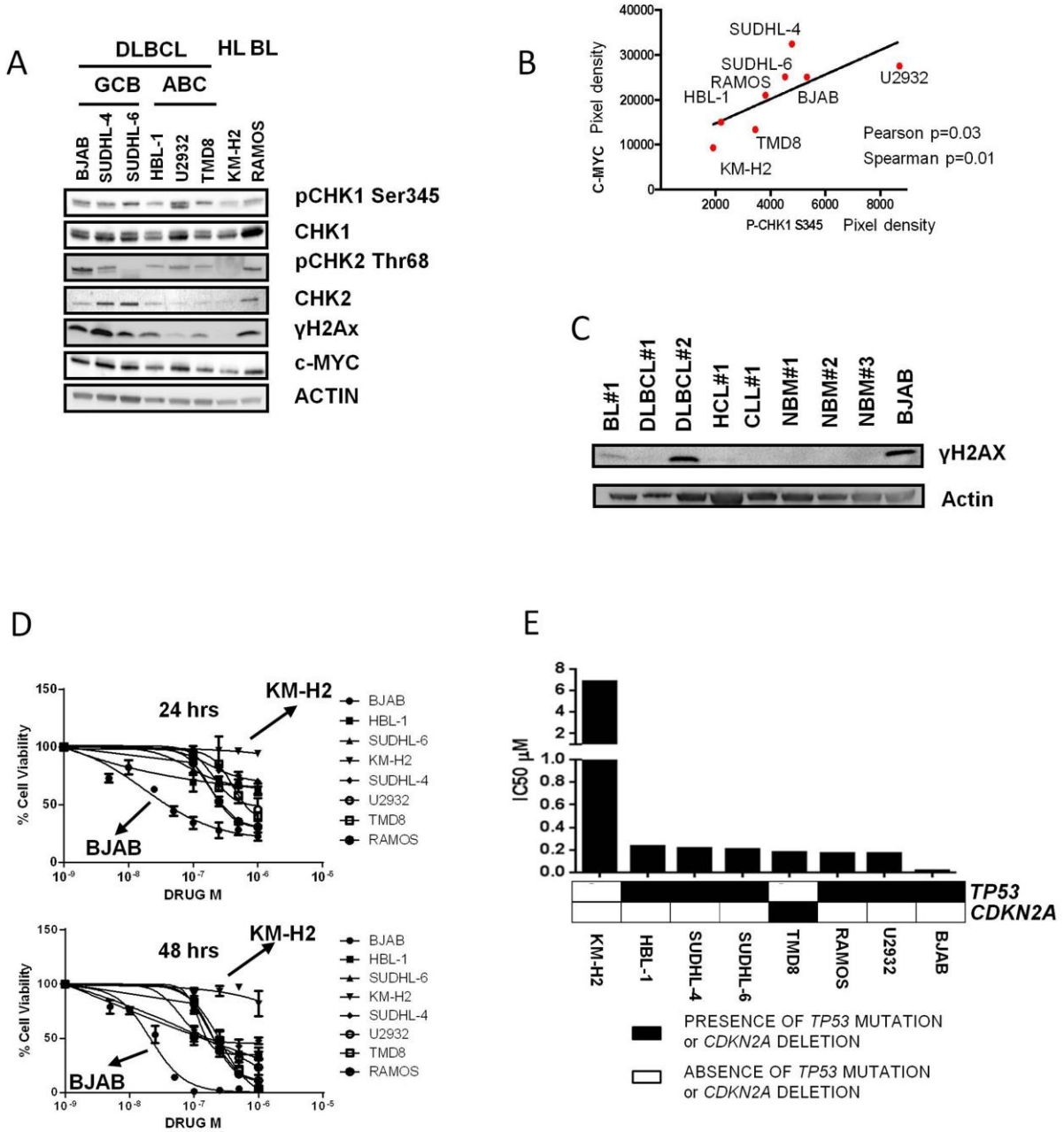
A
DLBCL
HL BL
GCB
ABC
BJAB
SUDHL-4
SUDHL-6
HBL-1
U2932
TMD8
KM-H2
RAMOS
pCHK1 Ser345
CHK1
pCHK2 Thr68
CHK2
γH2Ax
c-MYC
ACTIN
B
C-MYC Pixel density
P-CHK1 S345 Pixel density
Pearson p=0.03
Spearman p=0.01
C
BL#1
DLBCL#1
DLBCL#2
HCL#1
CLL#1
NBM#1
NBM#2
NBM#3
BJAB
γH2AX
Actin
D
% Cell Viability
DRUG M
24 hrs
48 hrs
KM-H2
BJAB
E
IC50 μM
TP53
CDKN2A
PRESENCE OF TP53 MUTATION or CDKN2A DELETION
ABSENCE OF TP53 MUTATION or CDKN2A DELETION

Fig. 3

A

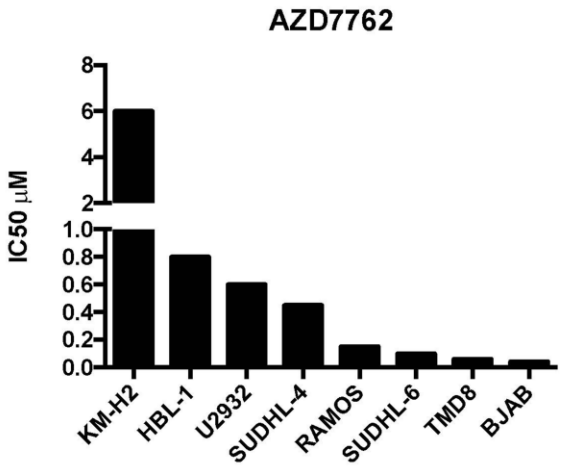

B

Cell line	Cell of origin	PF0477736 IC50 (nM)	AZD7762 IC50 (nM)
BJAB	GCB-DLBCL	9	40
U2932	ABC-DLBCL	160	600
RAMOS	BL	168	150
TMD8	ABC-DLBCL	180	60
SUDHL-6	GCB-DLBCL	200	100
SUDHL-4	GCB-DLBCL	210	450
HBL-1	ABC-DLBCL	230	800
KM-H2	HL	6800	6000

Figure 3. Antiproliferative activity of AZD7762 in our panel of B-cell lymphoma cell lines.

A) IC50 values after 48 hours of incubation with increasing doses of AZD7762.

B) Table showing 48 hours-IC50 values of PF-0477736 and AZD7762 in our panel of B-cell lymphoma cell lines.

Table 5. Detailed results of *TP53* mutations screening in cell lines and primary cells.

CELL LINE NAME	**DISEASE TYPE**	***TP53* MUTATION**	***CDKN2A* STATUS**
BJAB	GCB-DLBCL	H193R	WT
SUDHL-4	GCB-DLBCL	R273C	WT
SUDHL-6	GCB-DLBCL	Y234C	WT
HBL-1	ABC-DLBCL	V157A ex5	WT/LOSS
U-2932	ABC-DLBCL	C176Y ex5	WT
TMD8	ABC-DLBCL	WT	LOSS HOMOZYGOUS
RAMOS	BL	I254D ex7	WT
KM-H2	HL	WT	WT
PATIENT SAMPLES			
CLL#1	CLL	WT	WT
CLL#2	CLL	WT	WT
CLL#3	CLL	WT	WT
HCL#1	HAIRY CELL LEUKEMIA VARIANT	WT	WT
MZL#1	MARGINAL ZONE LYMPHOMA	WT	WT
DLBCL#1	DLBCL	WT	WT
DLBCL#2	DLBCL	WT	WT
BL#1	BURKITT LYMPHOMA	WT	WT
BL#2	BURKITT LYMPHOMA	R282W	WT
MCL#1	MANTLE CELL LYMPHOMA blastoid variant	WT	WT

Abbreviations: DLBCL (diffuse large B-cell lymphoma), GCB (germinal center), ABC (activated B-cell), BL (Burkitt lymphoma), HL (Hodgkin lymphoma), CLL (chronic B-cell lymphoid leukemia), HCL (Hairy cell leukemia), MZL (Marginal zone lymphoma), MCL (Mantle cell lymphoma), WT (wild type).

Fig. 4

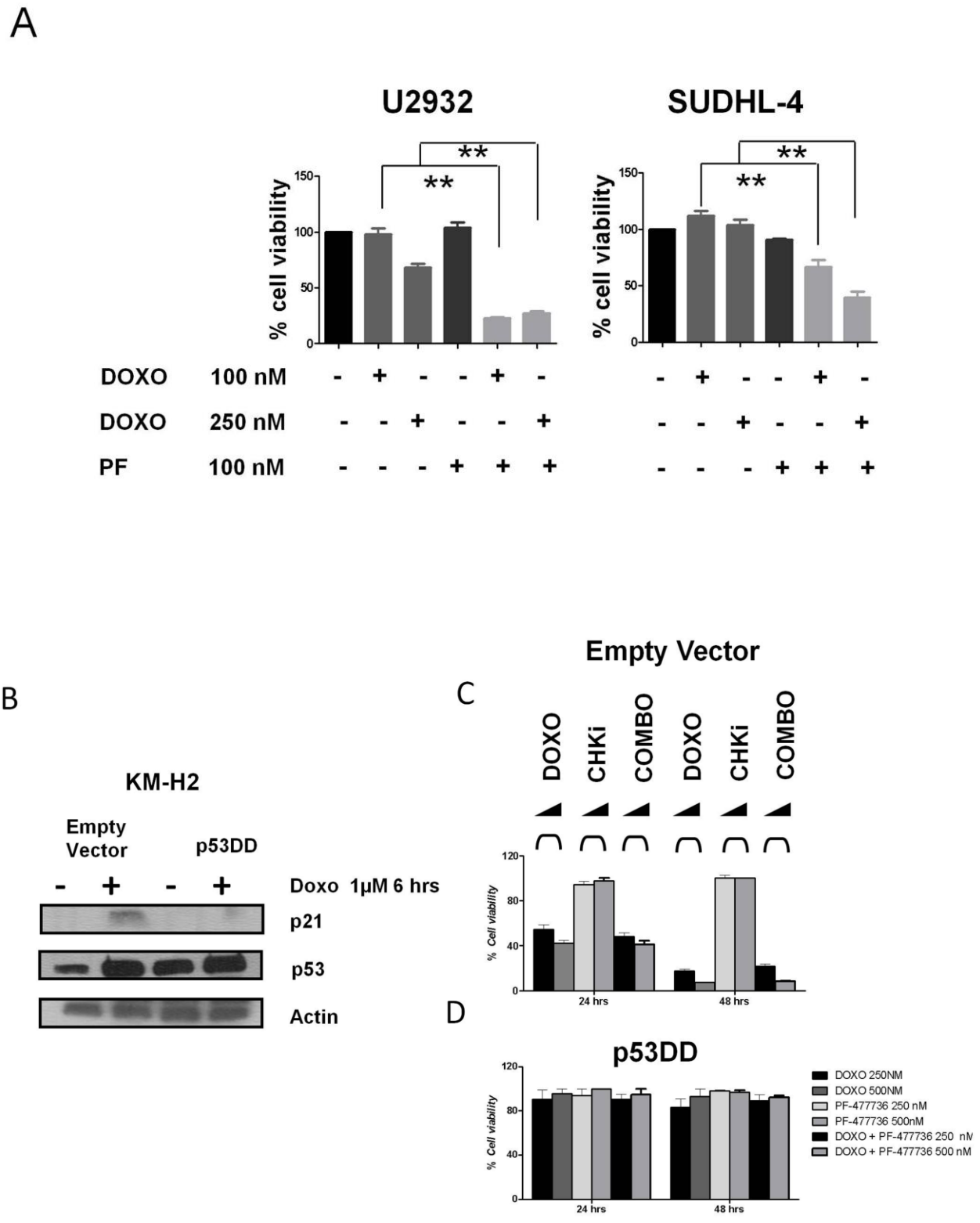
A
U2932
SUDHL-4
% cell viability
150
100
50
0
**
**
DOXO 100 nM - + - - + -
DOXO 250 nM - - + - - +
PF 100 nM - - - + + +
B
KM-H2
Empty Vector
p53DD
- + - +
Doxo 1μM 6 hrs
p21
p53
Actin
C
Empty Vector
DOXO
CHKi
COMBO
DOXO
CHKi
COMBO
% Cell viability
120
80
40
0
24 hrs
48 hrs
D
p53DD
% Cell viability
120
80
40
0
24 hrs
48 hrs
DOXO 250NM
DOXO 500NM
PF-477736 250 nM
PF-477736 500nM
DOXO + PF-477736 250 nM
DOXO + PF-477736 500 nM

Figure 4. P53 status and activity of CHK inhibitors in B-cell lymphoma.

A) PF-0477736 synergizes with Doxorubicin in TP53 mutant DLBCL cells.

WST-1 assay showing synergism between PF-0477736 (100 nM) and Doxorubicin (100 and 250 nM) after 48 hours of incubation in SUDHL-4 and U-2932 cells.

B) KM-H2 cells were transfected with a retroviral vector expressing the dominant negative *TP53* mutant (p53DD). The stable expression of this functionally inactive p53 mutant resulted in the accumulation of the p53 protein in p53 DD cells. KM-H2 cells transfected with p53DD and treated with Doxorubicin (Doxo) 1 μM for 6 hours lacked p21 expression, compared to empty retroviral vector (pBABE) transfected cells, which retained intact p53 function with normal transcription of p21 following doxorubicin exposure. These results confirm that KM-H2 cells were successfully transfected with the dominant negative p53 mutant p53DD.

C,D) KM-H2 cells transfected with empty retroviral vector (pBABE) or p53DD were incubated with doxorubicin (250 and 500 nM), PF-0477736 (250 and 500 nM) and the combination. Cells transfected with the empty vector were sensitive to Doxorubicin, resistant to PF-0477736 and the combination. Although as expected p53DD KM-H2 cells became resistant to Doxorubicin, they remained resistant to PF-0477736 and to the combination, both as 24 and at 48 hours. These findings demonstrate that at least in this cellular context disruption of p53 function is not sufficient to induce sensitivity to CHK inhibition. Each value is the mean of three independent experiments performed in triplicate. $^{*}P<0.05$; $^{**}P<0.005$; NS, not significant. Error bars represent s.e.m.

Fig. 5

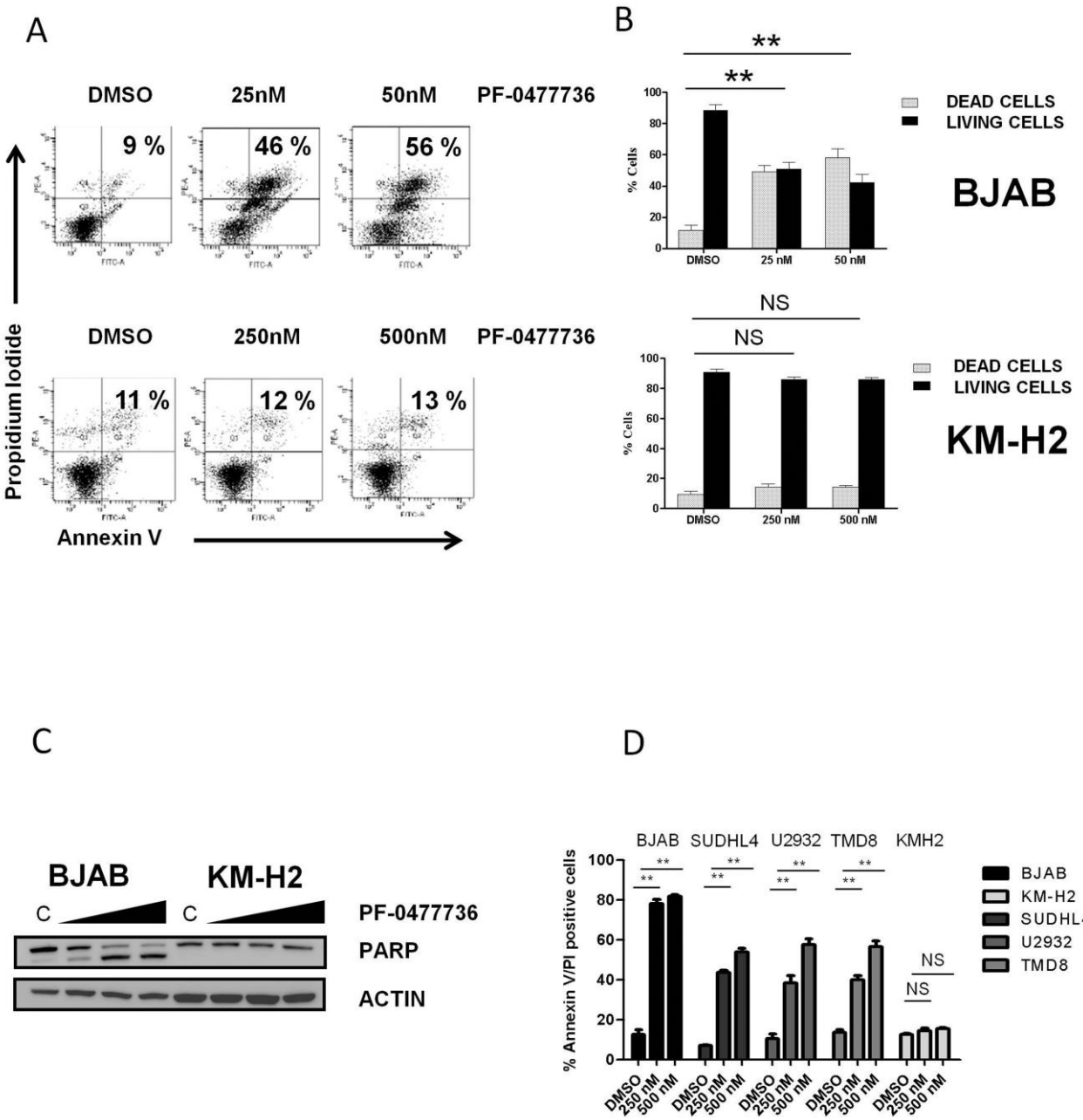
A
DMSO
25nM
50nM
PF-0477736
9 %
46 %
56 %
DMSO
250nM
500nM
PF-0477736
11 %
12 %
13 %
Propidium Iodide
Annexin V
B
**
**
% Cells
DEAD CELLS
LIVING CELLS
BJAB
DMSO
25 nM
50 nM
NS
NS
KM-H2
250 nM
500 nM
C
BJAB
KM-H2
C
PF-0477736
PARP
ACTIN
D
BJAB
SUDHL4
U2932
TMD8
KMH2
% Annexin V/PI positive cells
NS
NS

Figure 5. PF-0477736 induces cell death by apoptosis in DLBCL cell lines

A) Representative experiment demonstrating the effect of different doses of PF-0477736 (25 or 50 nM for 24 h in BJAB cells, 250 and 500 nM for 24 h in KM-H2 cells) on apoptosis as determined by annexin V-propidium iodide (PI) binding assay. The percentage of dead cells is shown in the upper right quadrant.

B) Summary of the results of dual annexin V and propidium iodide (PI) staining. Each value is the mean of three independent experiments performed in triplicate. Error bars represent s.e.m. $^{*}P<0.05$; $^{**}P<0.005$; NS (not significant).

C) Immunoblotting showing cleavage of poly (adenosine diphosphate ribose) polymerase (PARP) in BJAB cells after 24 hours of incubation with increasing doses (50, 250, 500 nM) of PF-0477736, with respect to control (C) (DMSO). Consistent the results of annexin V and propidium iodide staining no PARP cleavage was observed in the resistant KM-H2 cells following treatment.

D) Summary of the results of dual annexin V – (PI) staining for different DLBCL cell lines. Each value is the mean of three independent experiments performed in triplicate. Error bars represent s.e.m. $^{*}P<0.05$; $^{**}P<0.005$.

PF-0477736 inhibits CDC25c phosphorylation and determines rapid DNA damage accumulation in DLBCL cell lines.

Following DNA damage, the activation of CHK1 and CHK2 results in the inhibitory phosphorylation of the CDC25c phosphatase, which determines inhibition of mitotic entry, allowing DNA repair [13]. Therefore, the impairment of the G2/M checkpoint mediated by CHK inhibition should determine an uncontrolled DNA damage accumulation leading to replication fork collapse followed by cell death. To verify this hypothesis we first incubated the sensitive BJAB cells and the resistant KM-H2 cells with increasing concentrations of PF-0477736 and assessed effects on CDC25c and γH2AX phosphorylation. PF-0477736 potently inhibited the phosphorylation of CDC25c at ser 216 in the sensitive BJAB cells. As CDC25c de-phosphorylation triggers its proteasome dependent degradation, in line with recent findings [25] we also observed a decrease in total CDC25c levels following treatment. Moreover we observed a rapid and marked dose dependent increase of γH2AX consistent with accumulation of DNA damage (Figure 6 A,B). On the contrary, in KM-H2 cells we did not observe increased γH2AX levels following PF-0477736 treatment (western blot and immunofluorescence), and consistent with the low activation status of the DDR pathway, these cells did not show any constitutive CDC25c phosphorylation (Figure 6A). Taken together, these findings show that inhibition of the CHK kinases effectively increases the amount of DNA damage in DLBCL cells without the presence of exogenous genotoxic sources. In line with these results, incubation with PF-0477736 for 24 hrs triggered a futile feedback loop resulting in increased phosphorylation of ATM, and both its targets CHK1 and CHK2, as previously reported with different CHK inhibitors [26] (Figure 6C). The position and function of different components of the DDR pathway is briefly elucidated in figure 6D.

A similar mechanism resulting in DNA damage accumulation and hyper-phosphorylation of CHK1, was observed in all the DLBCL cell lines tested (Figure 6E)**.**

Fig. 6

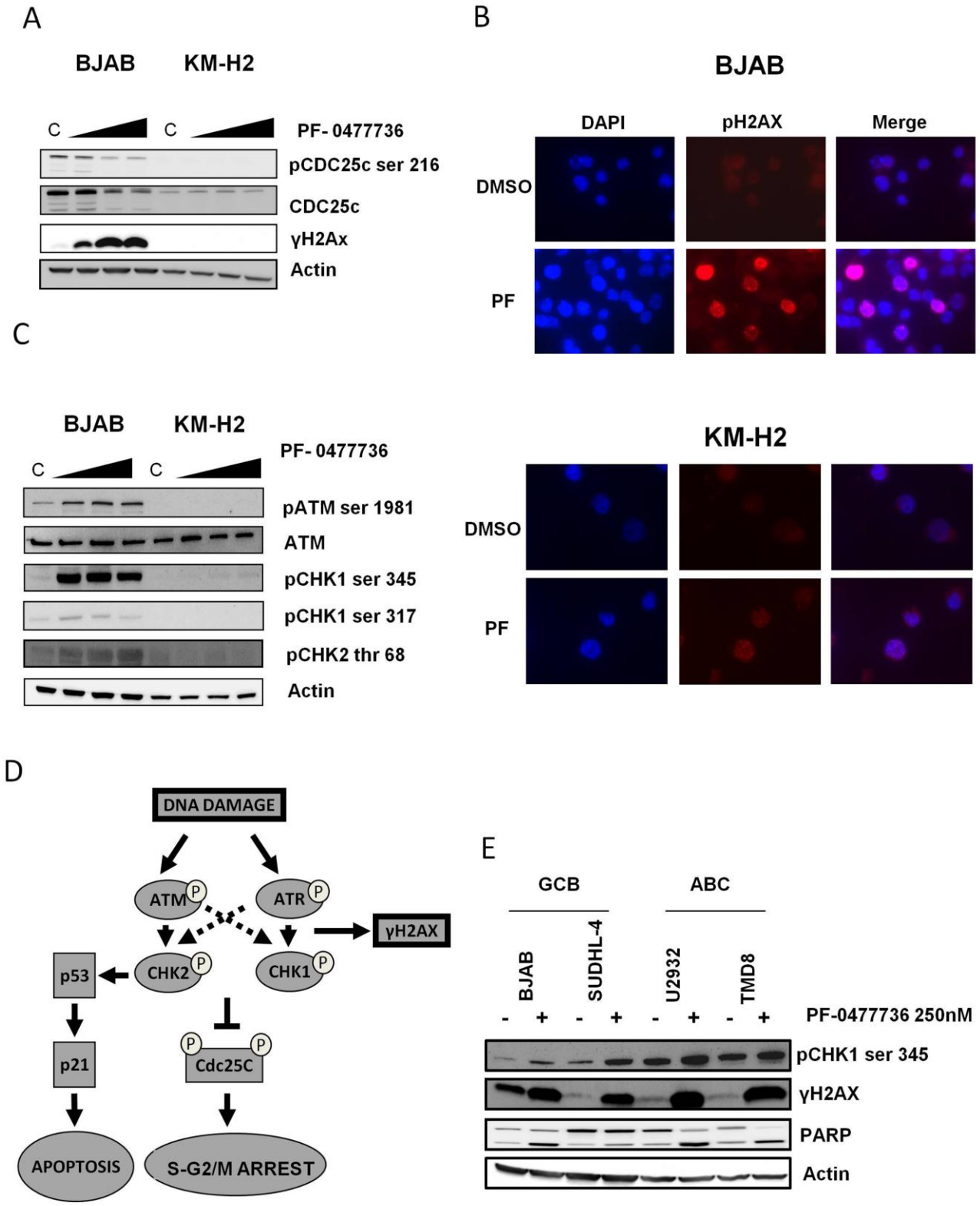
A
BJAB
KM-H2
C
C
PF- 0477736
pCDC25c ser 216
CDC25c
γH2Ax
Actin
B
BJAB
DAPI
pH2AX
Merge
DMSO
PF
C
BJAB
KM-H2
C
C
PF- 0477736
pATM ser 1981
ATM
pCHK1 ser 345
pCHK1 ser 317
pCHK2 thr 68
Actin
KM-H2
DMSO
PF
D
DNA DAMAGE
ATM
P
ATR
P
γH2AX
p53
CHK2
P
CHK1
P
p21
P
P
Cdc25C
APOPTOSIS
S-G2/M ARREST
E
GCB
ABC
BJAB
SUDHL-4
U2932
TMD8
- + - + - + - +
PF-0477736 250nM
pCHK1 ser 345
γH2AX
PARP
Actin

Figure 6. PF-0477736 inhibits CDC25c phosphorylation and determines DNA damage accumulation in DLBCL cells.

A) Western blot assay of BJAB and KM-H2 cells treated with increasing concentrations of PF-0477736 (50, 250, 500 nM) for 24 hours, showing inhibition of the donwstream target pCDC25c ser 216 and contemporary upregulation of the DNA damage marker γH2AX in the sensitive BJAB cells. On the contrary we could not detect any γH2AX induction in the resistant KM-H2 cells. Of note KM-H2 cells did not show any basal CDC25c phosphorylation, consistent with the low level of DDR activation shown in figure 1. C (control, DMSO).

B) Early effects of PF-0477736 on γH2AX phosphorylation levels.
Immunofluorescence of BIAB and KM-H2 cells indicating increased γH2AX levels as soon as after 3 hours of incubation with PF-0477736 (PF) 250 nM in the BJAB cells. Consistent with fig. 5A, the resistant KM-H2 cells did not show significant γH2AX upregulation following treatment.

C) Effects of PF-0477736 on the upstream components of the DDR pathway.
BJAB and KM-H2 cells were incubated with increasing concentrations of PF-0477736 (50, 250, 500 nM) for 24 hours and effects on ATM, CHK1 and CHK2 phosphorylation assessed by western blot. Consistent with DNA damage induction, PF-0477736 triggered a futile feedback loop in the sensitive BJAB cells, with increased ATM activation resulting in hyperphosphorylation of CHK1 and CHK2. C (control, DMSO).

D) Model of activation of the DDR pathway and G2/M checkpoint after DNA damage. After DNA damage, the histone H2AX is promptly recruited at the DNA damage foci and phosphorylated. The ATR and ATM kinases phosphorylate CHK1 and CHK2 which in turn phosphorylate the downstream target CDC25c phosphatase. This inhibitory phosphorylation results in cell cycle arrest, allowing DNA repair. The CHK2 kinase participates also in the G1/S checkpoint, by stabilizing p53 after DNA damage.

E) The GCB-derived SUDHL-4 cells and the ABC-derived U-2932 and TMD8 cells were incubated with PF-0477736 250 nM for 24 hours. BJAB cells were used as a control. Consistent with the data shown in fig. 5A and B, an induction of γH2AX and pCHK1 ser 345 was observed in all DLBCL cell lines. At the same time point, PARP cleavage consistent with apoptosis induction was detected in all DLBCL cell lines.

PF-0477736 shows high single agent activity and promotes DNA damage in primary aggressive B-cell lymphoma cells.

To investigate the activity of PF-0477736 in primary lymphoma cells and to evaluate its toxicity on bone marrow mononucleated cells we incubated a panel of primary cells from aggressive B-cell lymphoma patients (n=5) [2 BL, 2 DLBCL, 1 mantle cell lymphoma blastoid variant (MCL)], indolent B-cell lymphoma patients (n=5) (3 CLL, 1 MZL, 1 hairy cell leukemia) and normal bone marrow progenitors (n=7), with PF-0477736 at the fixed dose of 500 nM for 24 hours.

Consistently with our previous findings, aggressive B-cell lymphoma primary cells were sensitive to PF-0477736, whereas primary indolent B-cell lymphoma cells were only slightly sensitive and normal bone marrow progenitors were resistant (Figure 7A). Of note, in DLBCL primary cells PF-0477736 induced DNA damage accumulation with increase of γH2AX and pCHK1, as already demonstrated in DLBCL cell lines (Figure 7B). Characteristics of patients whose cells were used for *ex-vivo* experiments are shown in figure 7C.

PF-0477736 displayed activity both in *TP53* wild type and mutant primary cells, although the highest activity was observed in a *TP53* mutant Burkitt lymphoma sample (BL#2) (Figure 7B)(Table 5).

These data strongly suggest that PF-0477736 may exert a selective cytotoxic activity on aggressive lymphoma cells, without inducing specific changes in normal bone marrow mononucleated cells, at least in short term culture.

Fig. 7

A

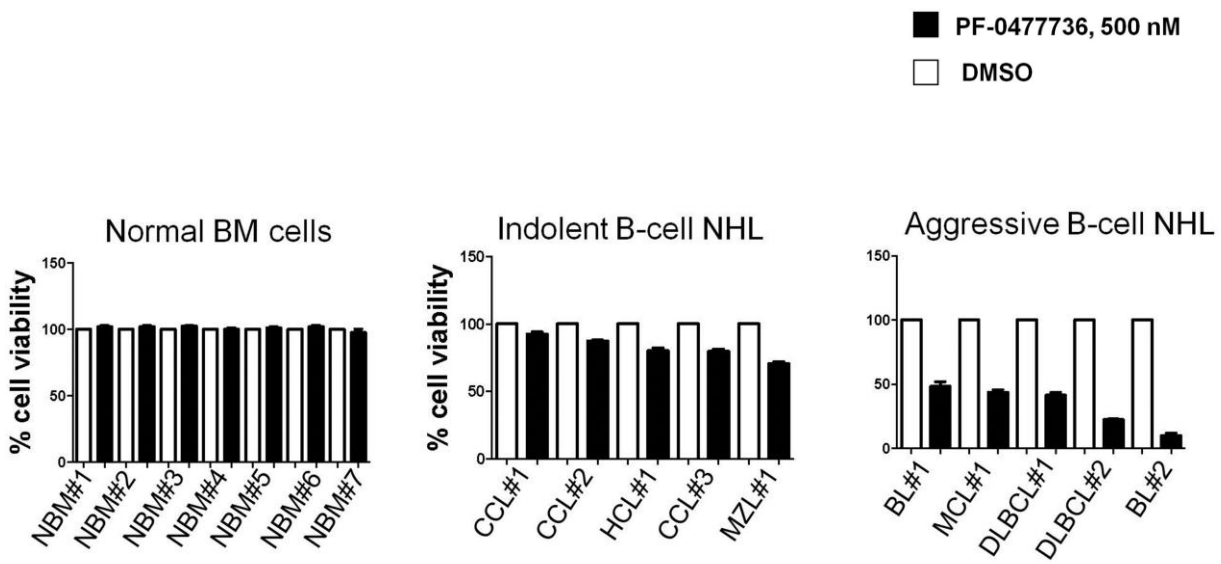
PF-0477736, 500 nM
DMSO
Normal BM cells
Indolent B-cell NHL
Aggressive B-cell NHL
% cell viability
150
100
50
0
NBM#1
NBM#2
NBM#3
NBM#4
NBM#5
NBM#6
NBM#7
CCL#1
CCL#2
HCL#1
CCL#3
MZL#1
BL#1
MCL#1
DLBCL#1
DLBCL#2
BL#2

B

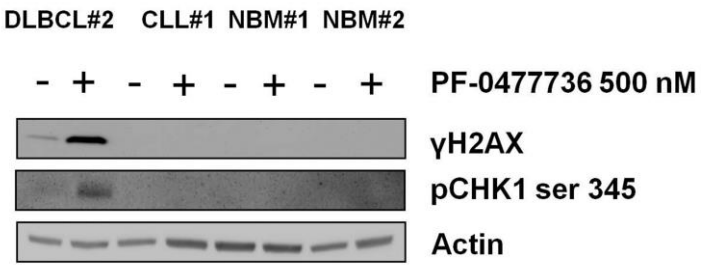
DLBCL#2
CLL#1
NBM#1
NBM#2
- + - + - + - +
PF-0477736 500 nM
γH2AX
pCHK1 ser 345
Actin

C

FACTOR	N°
Normal Bone Marrow	**7**
Age (Median; range)	**37 (20-68)**
Indolent NHL	**5**
Age (Median; range)	**59 (45-80)**
Chemonaive	**3**
CLL	**3**
HCL	**1**
MZL	**1**
Aggressive NHL	**5**
Age (Median; range)	**54 (28-78)**
Chemonaive	**3**
BL	**2**
DLBCL	**2**
ABC	**1**
GCB	**1**
MCL blastoid	**1**

Figure 7. Effects of PF-0477736 in primary lymphoma cells and bone marrow mononucleated cells.

A) Normal bone marrow mononucleated cells harvested from 7 patients with no signs of bone marrow involvement, at the moment of initial diagnosis, 5 primary indolent B-cell lymphoma samples, and 5 primary aggressive B-cell lymphoma samples were incubated with PF-0477736 500 nM for 24 hours, and cell viability evaluated by trypan-blue staining. The viability of each primary sample was normalized to its own untreated control. Error bars represent s.e.m. BL (Burkitt lymphoma), DLBCL (Diffuse large B-cell lymphoma), CLL (Chronic Lymphocytic Leukemia), HCL (Hairy Cell Leukemia), NBM (Normal bone marrow mononucleated cells), MZL (Marginal zone lymphoma), MCL (Mantle cell lymphoma).

B) Western blot assay showing on treatment modifications of γH2AX and pCHK1 ser 345 in primary cells. Similarly to what we observed in cell lines, treatment with PF-0477736 determined DNA damage accumulation with increased γH2AX and pCHK1 ser 345 levels in DLBCL primary cells, whereas no changes were observed in primary B-CLL cells and normal bone marrow mononucleated cells (NBM).

C) Table showing characteristics of patients whose primary cells were harvested and used for the experiments above.

Discussion

In this study we addressed the value of targeting the DDR pathway in aggressive B-cell lymphomas, focusing the attention on DLBCL. First we demonstrated that DLBCL is a neoplasm characterized by high inherent genomic instability and that the DDR pathway is aberrantly active in DLBCL cell lines, primary cells, and DLBCL tissue samples. In our patient cohort about half of all patients showed high levels of the DNA damage marker γH2AX and activation of the DDR components at the moment of initial diagnosis. We observed a significant correlation between γH2AX expression levels, constitutive DDR activation and c-MYC overexpression, suggesting an intimate relationship between *MYC*-induced oncogenic stress, genomic instability and DDR activation in DLBCL (Fig. 1E). Moreover, patients showing high γH2AX expression had a statistically significant lower 5-year OS compared to patients with low levels of γH2AX following conventional chemoimmunotherapy (Fig. 1C,D). These findings indicate that constitutive DDR activation could determine resistance to therapy with DNA damaging agents and that the DDR could be an important therapeutic target in DLBCL.

We demonstrated in *in vitro* and *ex-vivo* models that targeting the DDR pathway by inhibition of CHK kinases could be an effective treatment strategy in the subset of DLBCL with constitutive activation of DDR. Treatment with the CHK1/2 inhibitor PF-0477736 as single agent induced cell death by apoptosis at nanomolar concentrations in DDR positive DLBCL cell lines and markedly inhibited cell viability in primary DLBCL and BL cells. The antiproliferative affects observed with PF-0477736 in DLBCL cells were recapitulated by using a different inhibitor of CHK kinases (AZD7762), indicating a specific class effect of these compounds in DLBCL. Inhibition of CHK kinases effectively resulted in inhibition of the phosphorylation of the downstream target CDC25c, and increased the phosphorylation of the DNA damage marker γH2AX both in DLBCL cell lines and primary cells. Interestingly the increased amount of DNA damage determined by CHK inhibition triggered a futile feed-back loop characterized by enhanced ATM activation and

hyperphosphorylation of CHK1 and CHK2, which could be used as a biomarker of activity in future clinical trials. Notably we did not observe any *in vitro* cytotoxicity in normal bone marrow progenitors. Our results also indicate that the sensitivity to CHK inhibition of the DDR negative *TP53*-wild type KM-H2 cells was unaffected by transfection with the dominant negative p53 mutant p53DD, suggesting that the p53 status is not a primary determinant of sensitivity to DDR inhibition, and that the presence constitutive DDR activation likely plays a major role. On the other hand it is noteworthy that single agent PF-0477736 showed activity in *TP53* mutant aggressive B-cell lymphoma cell lines and primary cells, and that combined treatment with PF-0477736 was able to revert resistance to doxorubicin in *TP53* mutant cells (Figure 4). These observations suggest that inhibition of checkpoint kinases could be an effective treatment strategy for *TP53* mutant chemoresistant lymphomas with aberrantly active DDR pathway. These data are in line with previously published work showing single agent activity of CHK inhibitors in *MYC* driven lymphoma mouse models which recapitulate human Burkitt lymphoma [16], suggesting that Burkitt lymphoma and DLBCL share dysregulation of the DDR as a common pathogenetic feature. The role of DDR pathway and its upstream components [such as DNA dependent protein kinase (DNA-PK) and ATM] as therapeutic targets in *MYC* driven lymphomas has been confirmed in a recent report by Johnstone and coworkers on the efficacy of combined inhibition of ATM, DNA-PK and mammalian target of rapamycin (mTOR) in Eμ-MYC lymphoma models [27]. Intriguingly previous work from Blagosklonny and coworkers showed that enhanced DDR signaling was associated with mTOR over-activation during senescence coupled with hyper-mitogenic drive, and that inhibition of mTOR signaling by rapamycin attenuated DDR activation related to senescence [28,29]; since oncogene-induced replicative stress may lead to cellular senescence and DDR activation [30], and given that active mTOR signaling and c-MYC expression have been demonstrated to be significantly associated in DLBCL [31], it is tempting to think that mTOR and *MYC* may cooperate in inducing aberrant DDR activation, and that dual targeting of DDR and mTOR could be a valuable strategy in DLBCL.

Moreover it has been recently reported that inherent DNA damage is a common trait shared by a variety of haematological cancer cell lines of both myeloid and lymphoid origin [32]. These findings,

together with our observations, suggest that genomic instability, inherent DNA damage and alterations in DNA repair pathways may represent an Achilles heel by which highly genetically unstable aggressive lymphoid neoplasms may be targeted therapeutically.

Collectively, our observations depict a model of synthetic lethality in which cells with high oncogene induced genomic instability carry higher levels of constitutive DDR activation in order to cope with oncogene-induced replicative stress, and are thus sensitive to CHK inhibition, according to the oncogene-induced DNA damage model for cancer development proposed by Halozonetis and coworkers [11] (Figure 8). In conclusion, our data demonstrate that inherent genomic instability and DDR pathway constitutive activation are frequent features in DLBCL, and are associated with a poor prognosis. The high efficacy of CHK inhibitors in DLBCL cell lines and primary cells characterised by aberrantly active DDR pathway, strongly suggest that the constitutive activation of this pathway may represent a novel therapeutic target, providing a rationale for further clinical evaluation of this therapeutic strategy in DLBCL.

Fig. 8

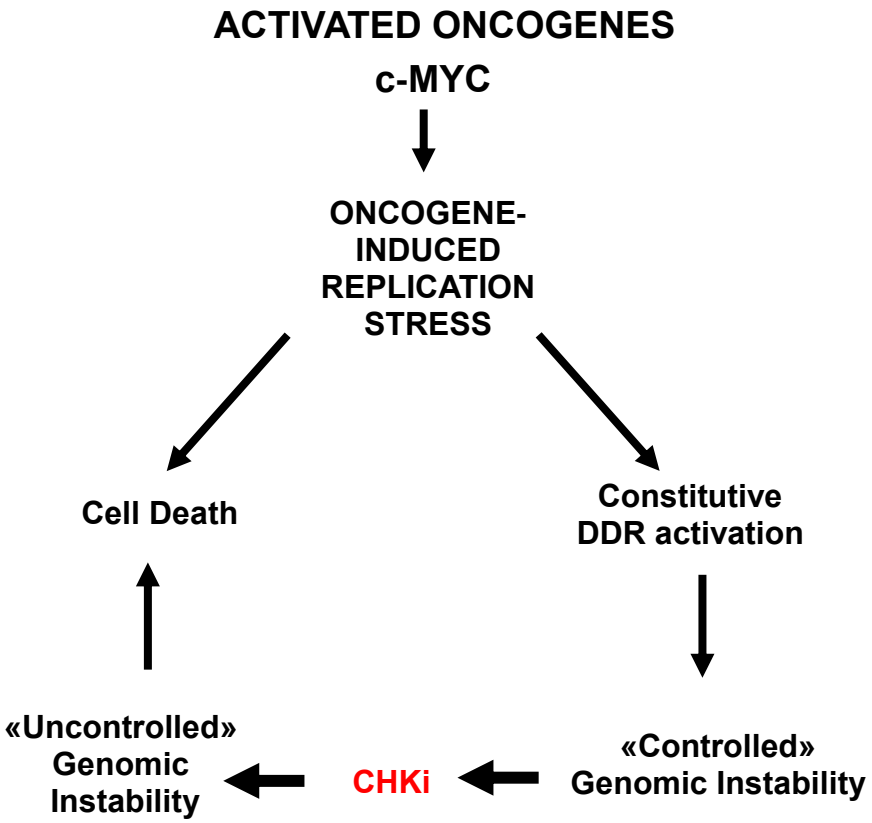

Figure 8. **Proposed model of oncogene induced genomic instability in DLBCL.**

Constitutive expression of oncogenes such as *MYC* increases replicative stress and determines G1/S checkpoint activation, which in normal cells leads to apoptotic cell death. Aggressive B-cell lymphoma cells tolerate increased amounts of genomic instability by constitutive activation of the G2/M checkpoint/DDR pathway (ATM-ATR-CHK1-CHK2-CDC25c axis). Inhibition of the DDR pathway by CHK inhibitors (CHKi) acts as a synthetic lethal mechanism, leading to “uncontrolled” genomic instability and cell death.

PART II

Intratumor heterogeneity for *TP53* mutational status at the moment of initial diagnosis in Burkitt lymphoma may drive therapy resistance and may be targeted with DNA-damage response pathway inhibitors.

Introduction

A phenomenon intimately related to genomic instability is intratumor heterogeneity, intended as the occurrence of genomic diversities within the same tumor. In fact, recent next generation sequencing (NGS) studies confirmed a high degree of genomic diversity through space (between different regions) and time (temporal patterns of evolution of different subclones) within the same tumors [33]. Since intratumor heterogeneity can directly affect response to treatment and outcome, these findings raise questions and concerns about the potential applications of NGS technologies in clinical practice for outcome prediction and therapy selection [34,35]. Adult sporadic BL is a rapidly progressing aggressive non-Hodgkin B-cell lymphoma subtype which often presents with abdominal masses [36]. Although with intensive chemoimmunotherapy the majority of adult BL patients can be cured, still 20-30% of cases are either primary refractory or relapse shortly after the completion of therapy, being exposed to uneffective and highly toxic chemotherapy regimens [36]. BL is characterized by high c-MYC expression due to the presence of *MYC* translocation which is a hallmark of the disease, and G1/S checkpoint dysfunction with frequent *TP53* mutations (30-40% of cases) [36]. The presence of *TP53* mutations drives chemoresistance in many different cancer models including B-cell lymphomas (49-51), and the cooperation between c-MYC overexpression and *TP53* mutations plays an important role in BL pathogenesis (52,53). Recently the genomic landscape of BL has been uncovered by next generation sequencing (NGS) studies and *TP53* confirmed to be among the 3 most recurrently mutated genes in BL (52,53).

Here we sought to define the mechanisms of chemoresistance in a 43-year old woman who was diagnosed with stage IVB bulky BL with massive abdominal effusion, who rapidly progressed and ultimately died of her disease despite therapy intensification. In this report we describe a

paradigmatic example of intratumor heterogeneity for the *TP53* mutational status at disease onset in BL. We performed deep targeted *TP53* sequencing of the bulky mass and of cells from the abdominal effusion, identifying 2 different subclones coexisting at the time of initial diagnosis: in fact the bulky mass was entirely *TP53* wild type whereas cells from abdominal effusion were *TP53* mutant, carrying an heterozygous R282W mutation. Furthermore we characterized the *TP53* mutant subclone by investigating the functional consequences of this mutation on chemotherapy response with an *ex-vivo* approach, confirming an impaired response to chemotherapy. We also demonstrated that the phenotype of this chemorefractory *TP53* mutant subclone was characterized by constitutive DDR activation and high *ex-vivo* sensitivity to inhibition of the DDR pathway, confirming the therapeutic potential of this strategy in *TP53* mutant, genomically unstable, aggressive lymphomas.

Results

Clinical Presentation

A 43-year-old woman was hospitalized in August 2011 in critical conditions with 2 bulky abdominal masses originating from both ovaries, a massive abdominal effusion and small bowel obstruction. Surgical biopsy of the bulky mass (left ovary), cytology of the malignant cells from ascitic fluid, and immunophenotype (CD10+, CD19+, CD20+, CD38+) led to the diagnosis of BL (Fig 1 A-E). Fluorescence in situ hybridization (FISH) on malignant cells from both bulky mass and ascitic fluid showed a t(8;22) chromosomal translocation involving the *MYC* locus. The principal comorbidity was a severe bipolar disorder and anorexia nervosa which was still active at the time of disease onset, so that the patient was severely underweight (body mass index < 17 kg/m^2) and deemed initially unfit for intensive chemotherapy (eastern cooperative oncology group performance status 4). The patient initially received 5 days of debulking cyclophosphamide (200 mg/m^2/die) followed by 1 CHOP (cyclophosphamide, doxorubicin, vincristine, prednisone) cycle (plus central nervous system prophylaxis), which was complicated by severe tumor lysis syndrome (TLS), and bowel perforation which required surgical intervention (Fig 1 F-I). A CT scan performed immediately after

the first chemotherapy cycle showed a marked reduction in the size of 2 abdominal bulky lesions, with persistence of the abdominal effusion (Fig 1 H). After recovering from surgery she received 2 additional Rituximab-CHOP-14 cycles but a CT scan performed right after showed marked disease progression (Fig 1 I). At this point the patient underwent therapy intensification according to the B-NHL-2002 regimen (56) but was completely unresponsive and ultimately died of rapidly progressing disease.

Fig. 1

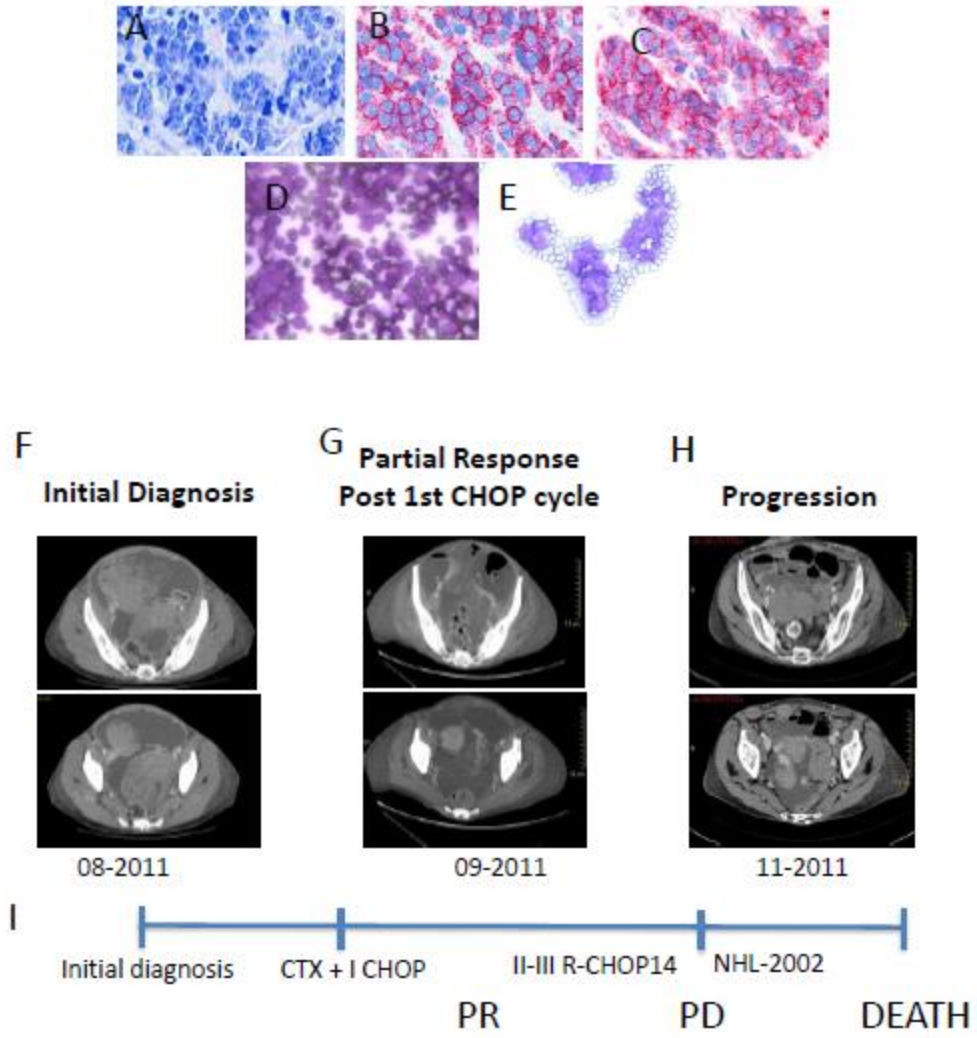

Figure 1. Clinical history and therapeutic interventions.

(A-E) Immunohistochemistry slides showing Burkitt lymphoma medium-sized cells (Giemsa stain) expressing CD10 (B) and CD20 (x400) (C). Peritoneal fluid collected at the moment of initial diagnosis (D, E), showing monomorphic BL cells with frequent mitotic figures.

(F-I) Clinical course of the patient depicted over a 4 months period with time points and different therapeutic interventions and CT scans performed at initial diagnosis (F), after first chemotherapy cycle (G), and at disease progression (H).

TP53 **sequencing and functional studies**

In order to investigate the mechanisms underlying resistance to standard and to intensive dose chemotherapy in this patient we performed deep *TP53* targeted DNA sequencing of the tumor tissue available from the initial biopsy (left ovary), of tumor cells initially collected from the ascitic fluid, and of matched normal saliva. The patient gave informed consent for the use of surplus tissue in research, and the protocol was approved by the Institutional Review Board. We found that the tumor tissue from the initial bulky mass was entirely *TP53* wild type, whereas lymphoma cells from the abdominal effusion harbored an heterozygous R282W mutation (Fig 2 A, B), which results in a 844C>T aminoacidic change and is known to negatively affect p53 function being associated to shorter survival in different cancer models (IARC database http://p53.iarc.fr/TP53GeneVariations.aspx) (57). These findings were confirmed by conventional sanger sequencing (Fig 2 C). Notably both samples were chemonaive being collected before the start of chemotherapy. These data depict an example of spatial intratumor heterogeneity for the *TP53* mutational status, in which 2 different lymphoma subclones (*TP53* wild type in the bulky mass and *TP53* mutant in ascitic fluid cells) coexisted at the moment of initial diagnosis. In order to define the impact of the R282W mutation on response to therapy in this specific case we treated the cultured *TP53* mutant primary BL cells from the ascitic fluid with either DMSO or doxorubicin 500 nM (Fig 3 A,B) for 24 hours. The *TP53* wild type Hodgkin lymphoma cell line KM-H2 was used as a control. According to the *TP53* mutational status primary BL cells were resistant to doxorubicin treatment, whereas the wild type KM-H2 cells were sensitive. Consistent with these data doxorubicin induced p21 expression in the KM-H2 cells but not in the primary BL cells (Fig 3C). These results confirm that the R282W mutation impairs p53 function determining a chemoresistant phenotype. Interestingly as shown in figure 1, while the *TP53* WT bulky masses rapidly responded to chemotherapy, the malignant *TP53* mutant ascites was still present at the time of CT scan despite multiple repeated paracenteses (Fig 1H), indicating a similar chemoresistant behavior also *in vivo*.

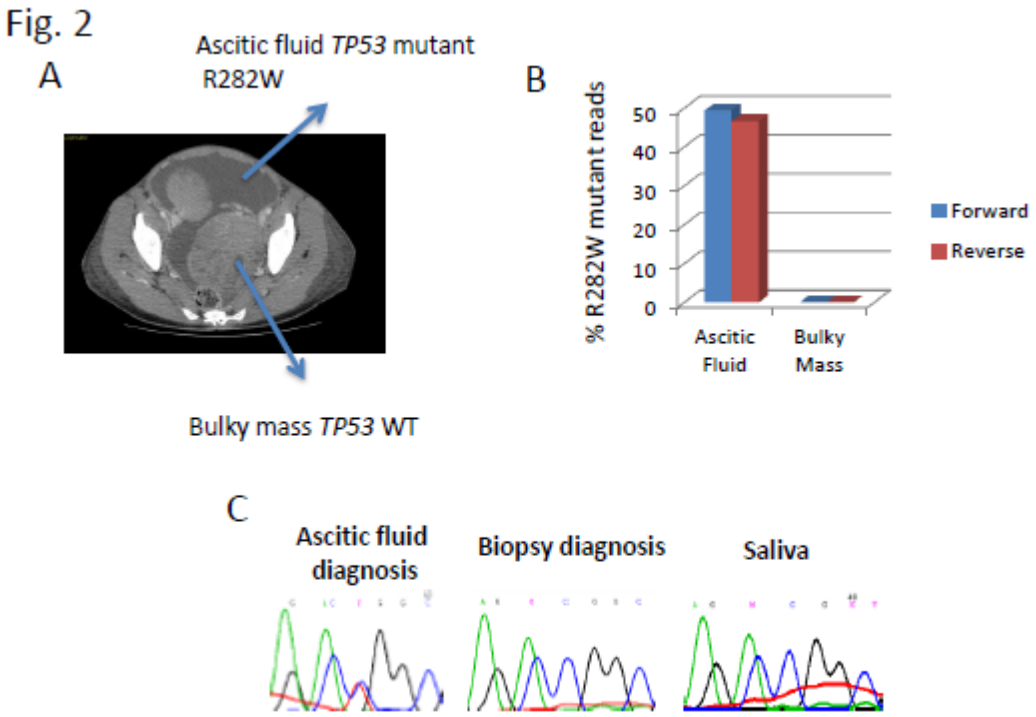

Figure 2. Intratumor heterogeneity for TP53 mutational status in BL.

(A,B) *TP53* deep targeted sequencing study of cells from the bulky mass and peritoneal fluid, showing the presence of R282W mutation in the peritoneal fluid cells but not in the bulky mass.

(C) Sanger sequencing analysis confirming the presence of an heterozygous R282W mutation in the cells from peritoneal fluid, and lack of mutation in the bulky mass.

Primary BL *TP53* mutant cells are sensitive to DDR inhibition

We then evaluated the expression levels of markers of genomic instability and DDR activation such as p-CHK1 ser 345 and γH2AX, in peritoneal fluid cells and in the bulky mass by western blotting (Fig. 3D) and immunohistochemistry (Fig. 3E-I). We found that peritoneal fluid cells demonstrated constitutive γH2AX and p-CHK1 S345 expression (Fig. 3D-F), confirming that these cells were characterized by genomic instability and constitutive activation of the DNA damage response pathway. The TP53 WT KM-H2 cells, used as negative control of DDR activation, were negative for both genomic instability markers (Fig 3D,G,H). Notably, although to a lesser extent, we observed positivity for these genomic instability markers also in the TP53 WT bulky mass (Fig. 3I,L). These data may suggest that the acquisition of genomic instability and of a DDR+ phenotype was an intrinsic feature of this neoplasm, that preceded the development of *TP53* mutation and the acquirement of a full chemoresitant phenotype. In order assess whether the *TP53* mutant subclone was sensitive to DDR inhibition we treated primary ascitic fluid cells and the *TP53 WT* KM-H2 cells (used as a negative control) with the CHK1 inhibitor PF-0477736, finding that BL peritoneal cells were exquisitely sensitive to CHK inhibition whereas KM-H2 cells were resistant (Fig 3M). Following CHK inhibition pH2AX S139 levels were increased in peritoneal fluid cells, indicating DNA damage accumulation. These data indicate that, consistently with the oncogene-induced replication stress model (11), in these cells the blockade of DDR leads to accumulation of endogenous DNA damage (Fig 3N). These data further confirm the relevance of constitutive DDR activation as possible therapeutic target in BL.

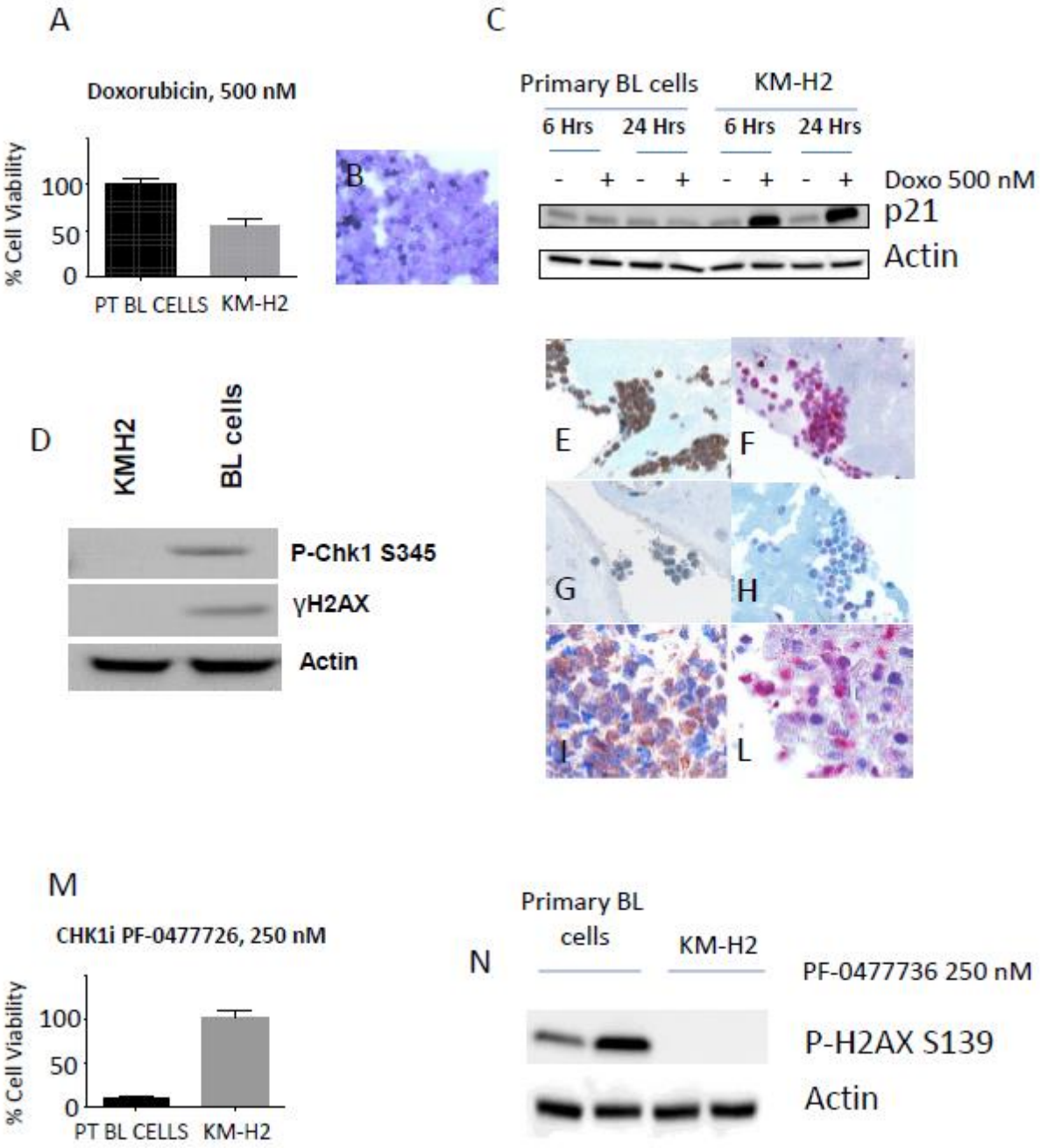
A
Doxorubicin, 500 nM
% Cell Viability
100
50
0
PT BL CELLS
KM-H2
B
C
Primary BL cells
KM-H2
6 Hrs
24 Hrs
6 Hrs
24 Hrs
- + - + - + - +
Doxo 500 nM
p21
Actin
D
KMH2
BL cells
P-Chk1 S345
γH2AX
Actin
E
F
G
H
I
L
M
CHK1i PF-0477726, 250 nM
% Cell Viability
100
50
0
PT BL CELLS
KM-H2
N
Primary BL cells
KM-H2
PF-0477736 250 nM
P-H2AX S139
Actin

Figure 3. Functional *ex vivo* studies showing doxorubicin resistance and sensitivity to DDR inhibition in *TP53* mutant cells from peritoneal effusion.

(A) WST-1 viability assay of primary BL cells and KM-H2 cells treated with DMSO and doxorubicin 500 nM for 24 hours. The percentage of viable cells after treatment in each cell line was normalized to its own untreated control

(B) Appearance of peritoneal fluid cells in culture.

(C) Western blot analysis of BL *TP53* mutant primary cells and *TP53* wild type HL-derived KM-H2 cells showing p21 induction in KM-H2 cells after doxorubicin treatment (500 nM for 6 and 24 hours)

(D) Western blot analysis of BL *TP53* mutant primary cells and *TP53* wild type HL-derived KM-H2 cells showing relative overexpression of pCHK1 S345 and pH2AX S139 in primary BL *TP53* mutant BL cells, compared to *TP53* wild type KM-H2 cells.

(E-H) Immunocytochemistry for p-CHK1 S345, p-H2AX S139, in cultured primary cells from peritoneal fluid (E,F), and KM-H2 cells (G,H) confirming western blot findings (x400).

(I,L) Representative immunohistochemistry slides showing p-CHK1 S345, p-H2AX S139 constitutive expression in the bulky mass (x400).

(M) WST-1 viability assay of primary BL cells and KM-H2 cells treated with DMSO and PF-0477736 250 nM for 24 hours. The percentage of viable cells after treatment in each cell line was normalized to its own untreated control.

(N) Western blot assay of BL *TP53* mutant primary cells and *TP53* wild type HL-derived KM-H2 cells showing pH2AX S139 induction in primary BL cells after PF-0477736 treatment (250 nM for 24 hours).

Discussion

To the best of our knowledge in this report we describe for the first time the occurrence of intratumor heterogeneity for the *TP53* mutational status in BL at the moment of initial diagnosis. The R282W mutation has already been described in hematologic tumors and has been found to be associated with poor outcome following chemotherapy in different cancer models (57). Although the prognostic significance of *TP53* mutations is already well established in several B-cell malignancies including diffuse large B-cell lymphoma (DLBCL) (35), such a role is not well defined in BL due to the small number of patients and treatment heterogeneity across different studies. Nevertheless, as a matter of fact, standard dose chemotherapy is less effective in BL compared to different B-cell lymphoma subtypes (48), possibly as a consequence of the higher incidence of *TP53* mutations. Moreover, specific *TP53* mutations have been associated with dismal outcome in BL (49), suggesting that *TP53* status indeed plays a role in determining response to chemotherapy in this disease. Even if initially our patient could not receive optimal intensive chemotherapy because of concomitant comorbidities and early therapy-related complications (TLS and bowel perforation), it should be noted that after the occurrence of chemoresistance the disease rapidly progressed despite subsequent treatment intensification. Furthermore we demonstrated with functional *ex-vivo* experiments that the *TP53* mutant cells from ascitic fluid were in fact resistant to doxorubicin, confirming an impaired p53-mediated response in these cells. Finally, the observation that the bulky *TP53* wild type mass initially responded to chemotherapy inducing TLS whereas the abdominal effusion persisted, suggests that the 2 clones were characterized in fact by differential chemosensitivity *in vivo*. The observation that *TP53* mutant cells from ascitic fluid overexpressed DDR activation markers and were sensitive to checkpoint kinase inhibition confirms that this therapeutic strategy could be of value in the treatment of MYC-driven *TP53* mutant aggressive lymphomas, and is consistent with a model in which c-MYC overexpression, together with the presence of *TP53* mutations and constitutive DDR activation cooperate in determining a highly aggressive chemoresistant phenotype in BL. Interestingly also the bulky *TP53* WT masses showed some evidence of DDR activation: this finding suggest that genomic instability and DDR activation

preceded the acquisition of the *TP53* mutation which leaded to a fully chemoresistant phenotype in this patient. Future studies should be aimed at testing DDR inhibitors alone or in combination with chemotherapy in aggressive B-cell lymphoma, with the goal of decreasing the intensity and thus the toxicity of current chemotherapy regimens, and possibly eradicating hidden *TP53* mutant subclones, which may drive chemotherapy resistance. As in this case the *TP53* mutant cells were able to proliferate in suspension in the peritoneal cavity, one could speculate that the advantage acquired by this subclone probably included increased metastatic potential and the capability to grow and expand independently from its original microenvironment, as described in different tumor models (26). In clinical practice, in case of aggressive lymphomas presenting with abdominal and pleural effusions could be important to investigate the *TP53* status both in the affected lymphnodes and in effusion cells, in order to rule out the occurrence of *TP53* mutations in cells which display different phenotypes and biologic behaviors. These observations could have broad implications especially when evaluating the possible applications of NGS technologies in clinical practice, both for outcome prediction and therapy selection. In the near future multiple tumor samples should be evaluated before tailoring therapies based on genome sequencing results. Moreover markers of constitutive DDR activation could be included in the diagnostic workup of aggressive B-cell lymphomas, in order to identify those patients whose tumors are more prone to genomic instability and consequently to develop intratumor heterogeneity. In other words the occurrence of intratumor heterogeneity for driver mutations potentially affecting the outcome and response to chemotherapy should be seriously taken in account at the moment of initial diagnosis, especially in aggressive lymphomas characterized by high expression levels of genomic instability markers. Finally these data suggest that intratumor heterogeneity for mutations affecting the G1/S checkpoint such as *TP53* mutations could be effectively targeted with DDR inhibitors, as single agents or in combination with chemotherapy.

Methods

Immunohistochemistry and primary tissues

Ten tissue microarrays (TMAs) were obtained from formalin-fixed paraffin-embedded samples collected at diagnosis from 3 reactive lymph nodes from 27 Chronic lymphocytic lymphoma/Small Lymphocytic lymphoma (CLL/SLL), 18 Splenic marginal zone lymphoma (SMZL), 22 Burkitt lymphoma (BL) and 44 classical Hodgkin lymphoma (CHL) cases and from 99 consecutive patients affected by DLBCL; the latter were classified in GCB (46 cases) and Non-GCB (53 cases) according to Hans algorithm [45]. All DLBCL cases were treated at our Institution with R-CHOP/CHOP-like regimens. All cases were retrieved from the archives of the Haematopathology Unit, Department of Experimental, Diagnostic and Specialty Medicine - DIMES, University of Bologna and were diagnosed from 2002 to 2011. The protocol was approved by the institutional review board of the University of Bologna. Informed consent was obtained from all patients. TMAs were constructed as previously reported [46]. TMAs sections were investigated by antibodies raised against fixation resistant epitopes of CHK1, p-CHK1 serine (ser) 345, CHK2, p-CHK2 threonine (thr) 68, CDC25, p-CDC25 ser 216, p-H2AX ser 319, c-MYC, BCL2, Ki67 and P53 proteins; the antibody reactivity and sources as well as the antigen retrieval protocols, dilutions and revelation systems are detailed in supplementary table S4. The cutoff for positivity was set at 30% of cells expressing the protein of interest, unless otherwise specified [46]. For Bcl-2 and c-MYC we applied a cut-off of 70% and 40%, whereas for p53 staining a cut-off of 50% was applied, according to the recent literature [9,47]. Immunohistochemical preparations were visualized and images were captured using Olympus Dot-slide microscope digital system equipped with the VS110 image analysis software.

Cell lines and primary cells

The human DLBCL-derived cell lines SUDHL-4, SUDHL-6, the HL cell line KM-H2 and the BL cell line RAMOS were obtained from the German Collection of Microorganisms and Cell Cultures, Department of Human and Animal Cell Cultures (Braunschweig, Germany). The DLBCL derived cell lines (HBL-1, U2932, TMD8, BJAB) were kindly provided by Dr. R.E. Davis (Houston, Tx). Cell lines were cultured in RPMI 1640 medium supplemented with 10% heat-inactivated fetal bovine serum (GIBCO BRL, Gaithersburg, MD), 1% L-glutamine, and penicillin-streptomycin in a humid environment of 5% CO_2 at 37°C. The phenotypes and genotypes of these cell lines have been previously described [48,49].

Primary cells from patients were obtained from bone marrow samples, peripheral blood of leukemic phase patients with more than 90% of circulating blasts, neoplastic abdominal and pleural effusions. Normal bone marrow progenitors were harvested from bone marrow aspirations performed in lymphoma patients undergoing initial staging procedures, which then resulted negative for lymphoma infiltration.

In vitro proliferation assay

Cells were seeded in 96-well plates at 50,000 cell/100 µl/well with increasing concentrations of drug (0.005-10 µM) for 24 and 48 hours. Cell viability was assessed by adding WST-1 reagent (Roche Applied Science, Basel, Switzerland) to the culture medium at 1:10 dilution, according to manufacturer`s instructions. Viability of primary cells was assessed by using the trypan blue staining, in triplicate experiments.

Statistical analyses

Survival analyses were performed using the Kaplan-Meier method and differences between groups calculated by using the log-rank test [50]. Multivariate analyses were performed by using the Cox regression model. Procedures to determine the effects of certain conditions on cell proliferation and apoptosis, were performed in 3 independent experiments. The 2-tailed Student *t* test was used to estimate the statistical significance of the differences between results from the 3 experiments. The Fisher`s exact test was used to estimate differences in proportions between groups. The

Pearson and Spearman's tests were used to establish correlations between different variables. Quantification of protein-band intensities by densitometric analysis was performed using NIH ImageJ software (National Institutes of Health, Bethesda, MD). The SPSS and PRISM softwares were used for the statistical analyses. Detailed methods are available in supplemental data.

Bioinformatic analysis of immunohistochemical (IHC) results.

To generate hierarchical clustering as displayed in dendrogram in Figure 1A, each antibody (p-CHK1 ser345, p-CHK2 Thr68, p-CDC25c ser216 and p-H2AX ser139) tested immunohistochemically was assigned a binary score value of either 0 or 1 depending on its positivity or negativity, respectively, in all cases studied. Furthermore, a relative frequency score [number of positive cases for a single IHC marker in a specific tumor (DLBCL, BL, cHL, SMZL, CLL) or normal tissue type (reactive lymph nodes) / total number of cases studied of the same tumor or normal tissue type] was calculated for each marker in all tumor subtypes and normal tissues studied. A matrix with the different tumor types and normal tissues types in rows and their IHC scores for the 4 markers in columns was created. Matrix data was analysed using MeV v4.7.4 tool [51]. Hierarchical cluster analysis was performed to classify different tumor types based on IHC marker expression. For every couple of tumor types and normal tissue type a and b, Euclidean distance D was calculated based on the expression of IHC markers as per the formula (i) $D_{ab} = \sqrt{\sum (a_i - b_i)^2}$. The tumor and normal types were furthermore clustered in different groups using a stepwise clustering method. For every step, tumor types or normal tissue type with minimal Euclidean distance were joined together in a cluster and the distance between different clusters was considered taking the maximum distance between 2 different elements each of them belonging to one of the two clusters (complete linkage method).

Western blotting, immunofluorescence and flow cytometry

Preparation of cellular protein lysates, protein quantitation, western immunoblotting and flow cytometry were performed as previously described [52,53]. A total of 30 μg of protein was denatured in Laemmli buffer at 95°C and separated by SDS-PAGE. Proteins were then electrotransferred onto nitrocellulose membranes and submitted to immunodetection with the relevant antibody. Membrane-bound secondary antibodies (HRP-conjugated goat anti-rabbit or anti-mouse, BioRad) were detected using SuperSignal West Dura Extended Duration Substrate (Pierce Chemical Co., Rockford, IL).

Immunofluorescence

Cells were seeded on poly-L-lysine coated glass coverslips and incubated overnight at 4°C. Samples were incubated for 1 hour in PBS plus 1% Bovine Serum Albumin (Sigma- Aldrich) to block unspecific binding before incubating with the primary antibody (Cell Signaling) diluted 1:400 in PBS 1% BSA overnight at 4°C. The samples were rinsed in PBS and then incubated with secondary antibody Alexa fluor 568 goat anti-rabbit IgG (Life Technologies) for 40 min at 37°C in darkness. Mounting and nuclei counterstaining were performed using the “pro long antifade reagent with DAPI” (Molecular Probes, Invitrogen) and observed under a fluorescence microscope.

Flow cytometry

Apoptosis was determined by using the Annexin V–FITC apoptosis detection kit (BD Pharmingen, San Diego, CA) according to the manufacturer’s instructions. Data were collected on a FACS Canto II flow cytometer (BD Biosciences, San Jose, CA) using FlowJo software (Tree Star, Ashland, OR).

Antibodies for western blotting, immunofluorescence and immunohistochemistry

For western blotting, antibodies to the following were purchased from Cell Signaling Technology: p-CHK1 ser 317, p-CHK1 ser 345, CHK1, pCHK2 thr 68, p-H2AX ser 139 (also used for immunofluorescence and imunohistochemistry), p-CDC25c ser 216, CDC25c, p-ATM ser 1981, ATM. C-MYC antibody was purchased from Abcam. For immunohistochemical studies, antibodies were obtained from Novus biologicals (CHK1, pCHK1ser 345, pCDC25 ser 216), Cell Signaling (Danvers, MA) (pCHK2 thr 68, p- H2AX ser 319), Epitomics (Burlingame, CA) (CHK2, CDC25, c-MYC), Menarini (Florence, Italy) (P53).

Reagents and proliferation assays

The CHK1/2 inhibitors PF-0477736 and AZD-7762 were purchased from Selleckchem (Houston, TX). Doxorubicin was purchased from Sigma Chemicals (Milan, Italy).

Production of KM-H2 -derived cells with stably inactivated p53

KM-H2 cells stably expressing p53DD, a truncated, dominant-negative form of murine p53 [54] and the related empty vector-transduced control cells (pBABE), were obtained as described by Morgenstern JP and Land H [55]. These cell lines were maintained in RPMI supplemented with 10% FBS and selected with puromycin antibiotic (Sigma-Aldrich, Milan, Italy).

Sanger sequencing of *TP53* and *CDKN2A/B* genes

Total cellular RNA was extracted using the RNeasy total RNA isolation kit (Qiagen, Valencia, CA). One microgram of total RNA was reverse transcribed using the M-MLV Reverse Transcriptase (Invitrogen, San Diego, CA). Three overlapping shorter amplicons [amplicon 1 (491 bp): exons 1-5; amplicon 2 (482 bp): exons 5-8; amplicon 3 (498 bp): exons 8-11)] covering the entire coding sequence (GenBank accession number NM_000546.4) were amplified with 2U of FastStart Taq DNA Polymerase (Roche Diagnostics, Mannheim, Germany), 0.8 mM dNTPs, 1 mM MgCl2, and

0.2 M forward and reverse primers (Table S2) in 25 µl reaction volumes. PCR products were purified using QIAquick PCR purification kit (Qiagen) and then directly sequenced using an ABI PRISM 3730 automated DNA sequencer (Applied Biosystems, Foster City, CA) and a Big Dye Terminator DNA sequencing kit (Applied Biosystems). All sequence variations were detected by comparison using the BLAST software tool (www.ncbi.nlm.nih.gov/BLAST/) to reference genome sequence data (GenBank accession number NM_000546.4).

Primer sequences. For each primer pair, the sequence (5'- 3'), the melting temperature (Tm), the length and the amplicon size are reported. Primers have been designed using Primer3 (v. 0.4.0) Software Tool. P53 F1 [(TGGATTGGCAGCCAGACT), Temperature (T) 60.36 C°, Length 18, Amplicon size 491 base pair (bp)], P53 R1 [(GGGGGTGTGGAATCAACC), T 61.01 C°, length 18, amplicon size 491 bp], P53 F2 [(TCAACAAGATGTTTTGCCAACT), T 59.50 C°, length 22, amplicon size 482 bp], P53 R2 [(GCGGAGATTCTCTTCCTCTGT), T 59.97 C°, length 21, amplicon size 482 bp], P53 F3 [(GGTAATCTACTGGGACGGAACA), T 60.24 C°, length 22, amplicon size 498 bp], P53 R3 [(CTATTGCAAGCAAGGGTTCAA), T 60.25 C°, length 21, amplicon size 498 bp]. For those cell lines with available data in the public domains, the *TP53* status found was in line with the informations available in the Cancer Cell Line Encyclopedia website (http://www.broadinstitute.org/ccle/home) for KM-H2, SUDHL-4 and SUDHL-6, in the IARC TP53 website (http://p53.iarc.fr/CellLines.aspx) for BJAB and RAMOS, and finally in the COSMIC database for U2932 (http://cancer.sanger.ac.uk/cancergenome/projects/cosmic/).

***CDKN2A/ARF and CDKN2B* mutation screening**

Genomic re-sequencing of all coding exons of *CDKN2A/ARF* and *CDKN2B* was performed in search of mutations using primers as previously described [56].

For each sample six amplicons were generated using Fast Start Taq DNA Polymerase protocol (Roche, Mannheim, Germany) and AmpliTaq Gold DNA Polymerase LD protocol (Applied Biosystems, Foster City, CA). Amplicons were thereafter purified using QIAquick PCR purification kit (Qiagen) and then directly sequenced using an ABI PRISM 3730 automated DNA sequencer

(Applied Biosystems) and a Big Dye Terminator DNA sequencing kit (Applied Biosystems). All sequence variations were detected by comparison using the BLAST software tool (www.ncbi.nlm.nih.gov/BLAST/) to reference genome sequence data (GenBank accession number NM_000077.4, NM_058195.3 e NM_004936, for *CDKN2A*, *ARF*, *CDKN2B*, respectively) obtained from the UCSC browser (http://genome.ucsc.edu/cgi-bin/hgGateway?db=hg18; March 2006 release).

CDKN2A/B **deletion analysis**

Deletions in *CDKN2A/B* genes were assessed using a Multiplex Ligation-dependent Probe Amplification (MLPA) approach and the SALSA MLPA kit P335 ALL (MRC-Holland) following manufacturer's recommendations (www.mlpa.com).

Ringraziamenti

Voglio ringraziare prima di tutto BolognAIL per il sostegno economico alla ricerca ed in particolare il Professor Sante Tura senza il supporto del quale questo studio non sarebbe stato possibile.

Il Professor Stefano Pileri, mio riferimento scientifico e relatore di questa tesi.

Il Professor Pier Luigi Zinzani per il costante supporto scientifico, fondamentale per la realizzazione ed il completamento di questo lavoro.

References

1- Morton LM, Wang SS, Devesa SS, Hartge P, Weisenburger DD, Linet MS. Lymphoma incidence patterns by WHO subtype in the United States, 1992-2001. Blood. 2006; 107: 265-76.

2- Ziepert M, Hasenclever D, Kuhnt E, Glass B, Schmitz N, Pfreundschuh M, Loeffler M. Standard International prognostic index remains a valid predictor of outcome for patients with aggressive CD20+ B-cell lymphoma in the rituximab era. J Clin Oncol. 2010; 28: 2373-80.

3- Rosenwald A, Wright G, Chan WC, Connors JM, Campo E, Fisher RI, Gascoyne RD, Muller-Hermelink HK, Smeland EB, Giltnane JM, Hurt EM, Zhao H, Averett L et al. The use of molecular profiling to predict survival after chemotherapy for diffuse large-B-cell lymphoma. N Engl J Med. 2002; 346: 1937-47.

4- Shipp MA, Ross KN, Tamayo P, Weng AP, Kutok JL, Aguiar RC, Gaasenbeek M, Angelo M, Reich M, Pinkus GS, Ray TS, Koval MA, Last KW et al. Diffuse large B-cell lymphoma outcome prediction by gene-expression profiling and supervised machine learning. Nat Med. 2002; 8: 68-74.

5- Alizadeh AA, Eisen MB, Davis RE, Ma C, Lossos IS, Rosenwald A, Boldrick JC, Sabet H, Tran T, Yu X, Powell JI, Yang L, Marti GE et al. Distinct types of diffuse large B-cell lymphoma identified by gene expression profiling. Nature. 2000; 403: 503-11.

6- Bakhoum SF, Danilova OV, Kaur P, Levy NB, Compton DA. Chromosomal instability substantiates poor prognosis in patients with diffuse large B-cell lymphoma. Clin Cancer Res. 2011; 17: 7704-11.

7- Pasqualucci L, Trifonov V, Fabbri G, Ma J, Rossi D, Chiarenza A, Wells VA, Grunn A, Messina M, Elliot O, Chan J, Bhagat G, Chadburn A et al. Analysis of the coding genome of diffuse large B-cell lymphoma. Nat Genet 2011; 43: 830-7.

8- Johnson NA, Slack GW, Savage KJ, Connors JM, Ben-Neriah S, Rogic S, Scott DW, Tan KL, Steidl C, Sehn LH, Chan WC, Iqbal J, Meyer PN et al. Concurrent expression of MYC and BCL2 in diffuse large B-cell lymphoma treated with rituximab plus cyclophosphamide, doxorubicin, vincristine, and prednisone. J Clin Oncol. 2012; 30: 3452-9.

9- Hu S, Xu-Monette ZY, Tzankov A, Green T, Wu L, Balasubramanyam A, Liu WM, Visco C, Li Y, Miranda RN, Montes-Moreno S, Dybkaer K, Chiu A et al. MYC/BCL2 protein coexpression contributes to the inferior survival of activated B-cell subtype of diffuse large B-cell lymphoma and demonstrates high-risk gene expression signatures: a report from The International DLBCL Rituximab-CHOP Consortium Program. Blood. 2013; 121: 4021-31.

10- Valera A, López-Guillermo A, Cardesa-Salzmann T, Climent F, González-Barca E, Mercadal S, Espinosa I, Novelli S, Briones J, Mate JL, Salamero O, Sancho JM, Arenillas L et al. MYC protein expression and genetic alterations have prognostic impact in diffuse large B-cell lymphoma treated with immunochemotherapy. Haematologica. 2013; 98: 1554-62.

11- Halazonetis TD, Gorgoulis VG, Bartek J. An oncogene-induced DNA damage model for cancer development. Science. 2008; 319: 1352-5.

12- Negrini S, Gorgoulis VG, Halazonetis TD. Genomic instability--an evolving hallmark of cancer. Nat Rev Mol Cell Biol. 2010;11:220-8.

13- Smith J, Tho LM, Xu N, Gillespie DA. The ATM-Chk2 and ATR-Chk1 pathways in DNA damage signaling and cancer. Adv Cancer Res. 2010; 108: 73-112.

14- Kinner A, Wu W, Staudt C, Iliakis G. Gamma-H2AX in recognition and signaling of DNA double-strand breaks in the context of chromatin. Nucleic Acids Res. 2008; 36: 5678-94.

15- Wu J, Clingen PH, Spanswick VJ, Mellinas-Gomez M, Meyer T, Puzanov I, Jodrell D, Hochhauser D, Hartley JA. γ-H2AX foci formation as a pharmacodynamic marker of DNA

damage produced by DNA cross-linking agents: results from 2 phase I clinical trials of SJG-136 (SG2000). Clin Cancer Res. 2013; 19: 721-30.

16- Ferrao PT, Bukczynska EP, Johnstone RW, McArthur GA. Efficacy of CHK inhibitors as single agents in MYC-driven lymphoma cells. Oncogene. 2012; 31: 1661-72.

17- Murga M, Campaner S, Lopez-Contreras AJ, Toledo LI, Soria R, Montaña MF, D'Artista L, Schleker T, Guerra C, Garcia E, Barbacid M, Hidalgo M, Amati B et al. Exploiting oncogene-induced replicative stress for the selective killing of Myc-driven tumors. Nat Struct Mol Biol. 2011; 18: 1331-5.

18- Höglund A, Nilsson LM, Muralidharan SV, Hasvold LA, Merta P, Rudelius M, Nikolova V, Keller U, Nilsson JA.. Therapeutic implications for the induced levels of Chk1 in Myc-expressing cancer cells. Clin Cancer Res. 2011; 17: 7067-79.

19- De Miranda NF, Peng R, Georgiou K, Wu C, Falk Sörqvist E, Berglund M, Chen L, Gao Z, Lagerstedt K, Lisboa S, Roos F, van Wezel T, Teixeira MR et al. DNA repair genes are selectively mutated in diffuse large B cell lymphomas. J Exp Med. 2013; 210: 1729-42.

20- Carrassa L, Damia G. Unleashing Chk1 in cancer therapy. Cell Cycle. 2011;10:2121-8.

21- Karp JE, Thomas BM, Greer JM, Sorge C, Gore SD, Pratz KW, Smith BD, Flatten KS, Peterson K, Schneider P, Mackey K, Freshwater T, Levis MJ et al. Phase I and pharmacologic trial of cytosine arabinoside with the selective checkpoint 1 inhibitor Sch 900776 in refractory acute leukemias. Clin Cancer Res. 2012; 18: 6723-31.

22- Blasina A, Hallin J, Chen E, Arango ME, Kraynov E, Register J, Grant S, Ninkovic S, Chen P, Nichols T, O'Connor P, Anderes K.. Breaching the DNA damage checkpoint via PF-00477736, a novel small-molecule inhibitor of checkpoint kinase 1. Mol Cancer Ther. 2008; 7: 2394-404.

23- Zhang C, Yan Z, Painter CL, Zhang Q, Chen E, Arango ME, Kuszpit K, Zasadny K, Hallin M, Hallin J, Wong A, Buckman D, Sun G et al. PF-00477736 mediates checkpoint kinase 1 signaling pathway and potentiates docetaxel-induced efficacy in xenografts. Clin Cancer Res. 2009; 15: 4630-40.

24- Landau HJ, McNeely SC, Nair JS, Comenzo RL, Asai T, Friedman H, Jhanwar SC, Nimer SD, Schwartz GK.. The checkpoint kinase inhibitor AZD7762 potentiates chemotherapy-induced apoptosis of p53-mutated multiple myeloma cells. Mol Cancer Ther. 2012; 11: 1781-8.

25- Thanasoula M, Escandell JM, Suwaki N, Tarsounas M. ATM/ATR checkpoint activation downregulates CDC25C to prevent mitotic entry with uncapped telomeres. EMBO J. 2012; 31: 3398-410.

26- Parsels LA, Qian Y, Tanska DM, Gross M, Zhao L, Hassan MC, Arumugarajah S, Parsels JD, Hylander-Gans L, Simeone DM, Morosini D, Brown JL, Zabludoff SD et al. Assessment of chk1 phosphorylation as a pharmacodynamic biomarker of chk1 inhibition. Clin Cancer Res. 2011; 17: 3706-15.

27- Shortt J, Martin BP, Newbold A, Hannan KM, Devlin JR, Baker AJ, Ralli R, Cullinane C, Schmitt CA, Reimann M, Hall MN, Wall M, Hannan RD, Pearson RB, McArthur GA, Johnstone RW. Combined inhibition of PI3K-related DNA damage response kinases and mTORC1 induces apoptosis in MYC-driven B-cell lymphomas. Blood. 2013; 121 :2964-74.

28- Pospelova TV, Demidenko ZN, Bukreeva EI, Pospelov VA, Gudkov AV, Blagosklonny MV. Pseudo-DNA damage response in senescent cells. Cell Cycle. 2009;8:4112-8.

29- Leontieva OV, Lenzo F, Demidenko ZN, Blagosklonny MV. Hyper-mitogenic drive coexists with mitotic incompetence in senescent cells. Cell Cycle. 2012;11:4642-9.

30- Darzynkiewicz Z. When senescence masquerades as DNA damage: is DNA replication stress the culprit? Cell Cycle. 2009;8:3810-1.

31- Pourdehnad M, Truitt ML, Siddiqi IN, Ducker GS, Shokat KM, Ruggero D. Myc and mTOR converge on a common node in protein synthesis control that confers synthetic lethality in Myc-driven cancers. Proc Natl Acad Sci U S A. 2013;110:11988-93.

32- Cottini F, Hideshima T, Xu C, Sattler M, Dori M, Agnelli L, Hacken E, Bertilaccio MT, Antonini E, Neri A, Ponzoni M, Marcatti M, Richardson PG, Carrasco R, Kimmelman AC, Wong KK, Caligaris-Cappio F, Blandino G, Kuehl WM, Anderson KC, Tonon G. Rescue of

Hippo coactivator YAP1 triggers DNA damage-induced apoptosis in hematological cancers. Nat Med. 2014; 20 :599-606.

33- Gerlinger M, Rowan AJ, Horswell S, Larkin J, Endesfelder D, Gronroos E, et al. Intratumor heterogeneity and branched evolution revealed by multiregion sequencing. N Engl J Med. 2012 Mar 8;366(10):883-92.

34- Almendro V, Cheng YK, Randles A, Itzkovitz S, Marusyk A, Ametller E, et al. Inference of tumor evolution during chemotherapy by computational modeling and in situ analysis of genetic and phenotypic cellular diversity. Cell Rep. 2014;6(3):514-27.

35- Zhao B, Hemann MT, Lauffenburger DA. Intratumor heterogeneity alters most effective drugs in designed combinations. Proc Natl Acad Sci U S A. 2014;111(29):10773-8.

36- Molyneux EM, Rochford R, Griffin B, Newton R, Jackson G, Menon G, Harrison CJ,Israels T, Bailey S. Burkitt's lymphoma. Lancet. 2012;379(9822):1234-44.

37- Klumb CE, Furtado DR, de Resende LM, Carriço MK, Coelho AM, de Meis E, et al. DNA sequence profile of TP53 gene mutations in childhood B-cell non-Hodgkin's lymphomas: prognostic implications. Eur J Haematol. 2003;71(2):81-90.

38- Hemann MT, Bric A, Teruya-Feldstein J, Herbst A, Nilsson JA, Cordon-Cardo C, et al. Evasion of the p53 tumour surveillance network by tumour-derived MYC mutants. Nature. 2005;436(7052):807-11.

39- Rowh MA, DeMicco A, Horowitz JE, Yin B, Yang-Iott KS, Fusello AM et al. Tp53 deletion in B lineage cells predisposes mice to lymphomas with oncogenic translocations. Oncogene. 2011;30(47):4757-64.

40- Love C, Sun Z, Jima D, Li G, Zhang J, Miles R, et al. The genetic landscape of mutations in Burkitt lymphoma. Nat Genet. 2012;44(12):1321-5.

41- Schmitz R, Young RM, Ceribelli M, Jhavar S, Xiao W, Zhang M, Wright G, et al. Burkitt lymphoma pathogenesis and therapeutic targets from structural and functional genomics. Nature. 2012;490(7418):116-20.

42- Intermesoli T, Rambaldi A, Rossi G, Delaini F, Romani C, Pogliani EM, et al. High cure rates in Burkitt lymphoma and leukemia: a Northern Italy Leukemia Group study of the

German short intensive rituximab-chemotherapy program. Haematologica. 2013 Nov;98(11):1718-25.

43- Xu J, Wang J, Hu Y, Qian J, Xu B, Chen H, et al. Unequal prognostic potentials of p53 gain-of-function mutations in human cancers associate with drug-metabolizing activity. Cell Death Dis. 2014 Mar 6;5:e1108.

44- Schwitalla S, Ziegler PK, Horst D, Becker V, Kerle I, Begus-Nahrmann Y, et al. Loss of p53 in enterocytes generates an inflammatory microenvironment enabling invasion and lymph node metastasis of carcinogen-induced colorectal tumors. Cancer Cell. 2013;23:93-106.

45- Hans CP, Weisenburger DD, Greiner TC, Gascoyne RD, Delabie J, Ott G, Müller-Hermelink HK, Campo E, Braziel RM, Jaffe ES, Pan Z, Farinha P, Smith LM et al. Confirmation of the molecular classification of diffuse large B-cell lymphoma by immunohistochemistry using a tissue microarray. Blood. 2004; 103: 275-82.

46- Went P, Agostinelli C, Gallamini A, Piccaluga PP, Ascani S, Sabattini E, Bacci F, Falini B, Motta T, Paulli M, Artusi T, Piccioli M, Zinzani PL et al. Marker expression in peripheral T-cell lymphoma: a proposed clinical-pathologic prognostic score. J Clin Oncol. 2006; 24: 2472–2479.

47- Xu-Monette ZY, Wu L, Visco C, Tai YC, Tzankov A, Liu WM, Montes-Moreno S, Dybkaer K, Chiu A, Orazi A, Zu Y, Bhagat G, Richards KL et al. Mutational profile and prognostic significance of TP53 in diffuse large B-cell lymphoma patients treated with R-CHOP: report from an International DLBCL Rituximab-CHOP Consortium Program Study. Blood. 2012; 120: 3986-96.

48- Drexler HG. Recent results on the biology of Hodgkin and Reed-Sternberg cells. II. Continuous cell lines. Leuk Lymphoma. 1993 ;9:1-25.

49- Davis RE, Ngo VN, Lenz G, Tolar P, Young RM, Romesser PB, Kohlhammer H, Lamy L, Zhao H, Yang Y, Xu W, Shaffer AL, Wright G et al: Chronic active B-cell-receptor signalling in diffuse large B-cell lymphoma. Nature 2010, 463: 88-92.

50- Kaplan EL, Meier P. Nonparametric estimations from incomplete observations. J Amer Statist Assn .1958; 53:457-81.

51- Saeed AI, Sharov V, White J, et al. TM4: a free, open-source system for microarray data management and analysis. Biotechniques. 2003; 34(2): 374-378.

52- Derenzini E, Lemoine M, Buglio D, Katayama H, Ji Y, Davis RE, Sen S, Younes A.. The JAK inhibitor AZD1480 regulates proliferation and immunity in Hodgkin lymphoma. Blood Cancer J. 2011;1:e46.

53- Lemoine M, Derenzini E, Buglio D, Medeiros LJ, Davis RE, Zhang J, Ji Y, Younes A. The pan-deacetylase inhibitor panobinostat induces cell death and synergizes with everolimus in Hodgkin lymphoma cell lines. Blood. 2012; 119: 4017-25.

54- Shaulian E, Haviv I, Shaul Y, Oren M. Transcriptional repression by the C-terminal domain of p53. Oncogene 1995; 10: 671-80.

55- Morgenstern JP, Land H. A series of mammalian expression vectors and characterisation of their expression of a reporter gene in stably and transiently transfected cells. Nucleic Acids Res 1990; 18: 1068.

56- Iacobucci I, Ferrari A, Lonetti A, et al. CDKN2A/B alterations impair prognosis in adult BCR-ABL1-positive acute lymphoblastic leukemia patients. Clin Cancer Res. 2011;17(23):7413-23.